Journal of Computational Physics 228 (2009) 833–860

Contents lists available at ScienceDirect

Journal of Computational Physics

journal homepage: www.elsevier.com/locate/jcp

Dissipative issue of high-order shock capturing schemes with non-convex equations of state

Olivier Heuzé, Stéphane Jaouen *, Hervé Jourdren

CEA/DAM-Île de France, Bruyères-le-Châtel, F-91297 Arpajon Cedex, France

ARTICLE INFO

Article history:
Received 20 December 2007
Received in revised form 29 September 2008
Accepted 4 October 2008
Available online 15 October 2008

Keywords:
Compressible fluid dynamics
Non-convex equation of state
Fundamental derivative
Riemann problem
Composite waves
High-order schemes
vNR-type methods
Godunov-type methods
Artificial viscosity
Flux limiters

ABSTRACT

It is well known that, closed with a non-convex equation of state (EOS), the Riemann problem for the Euler equations allows non-standard waves, such as split shocks, sonic isentropic compressions or rarefaction shocks, to occur. Loss of convexity then leads to non-uniqueness of entropic or Lax solutions, which can only be resolved via the Liu-Oleinik criterion (equivalent to the existence of viscous profiles for all admissible shock waves). This suggests that in order to capture the physical solution, a numerical scheme must provide an appropriate level of dissipation. A legitimate question then concerns the ability of high-order shock capturing schemes to naturally select such a solution. To investigate this question and evaluate modern as well as future high-order numerical schemes, there is therefore a crucial need for well-documented benchmarks. A thermodynamically consistent $\mathscr{C}^\infty$ non-convex EOS that can be easily introduced in Eulerian as well as Lagrangian hydrocodes for test purposes is here proposed, along with a reference solution for an initial value problem exhibiting a complex composite wave pattern (the Bizarrium test problem). Two standard Lagrangian numerical approaches, both based on a finite volume method, are then reviewed (vNR and Godunov-type schemes) and evaluated on this Riemann problem. In particular, a complete description of several *state-of-the-art* high-order Godunov-type schemes applicable to general EOSs is provided. We show that this particular test problem reveals quite severe when working on high-order schemes, and recommend it as a benchmark for devising new limiters and/or next-generation highly accurate schemes.

1. Introduction

This study deals with Euler equations and systems of conservation laws (SCL). It is well known that SCLs must be closed by constitutive relations that characterize the thermodynamical properties of the considered materials. Concerning the Euler equations, such relations are embodied in the definition of the specific internal energy ε as a function of the specific volume τ and entropy S, which defines an equation of state (EOS) in complete form. Indeed, all other thermodynamical parameters can be deduced from this relation (as an example, the pressure p and temperature T are implicitely defined by the Gibbs relation $TdS = d\varepsilon + pd\tau$). As was noticed by Jouguet [23], we will see throughout this study that of particular importance is the sign of one of these parameters, namely according to Thompson's terminology [43] the *fundamental derivative* $\mathscr{G}$. This thermodynamical function, whose definition will be recalled in the next section, measures the convexity of isentropes in the (p,τ)-plane. Retaining Wendroff's terminology [47,48], we will refer as a non-convex EOS, an EOS such that this fundamental derivative may become negative. Be aware that such a definition of non-convex EOS may be misleading. Indeed, thermodynamic stability requires that $\varepsilon(\tau,S)$ is a convex function of its arguments [3,6] – implying by the way that the

* Corresponding author.
E-mail address: stephane.jaouen@cea.fr (S. Jaouen).

0021-9991/$ - see front matter © 2008 Elsevier Inc. All rights reserved.
doi:10.1016/j.jcp.2008.10.005

system of conservation laws is hyperbolic – and throughout this work we will always assume that this latter property is satisfied.

To understand the wave structure as well as to devise numerical schemes to compute solutions to SCLs, a preliminary step consists in the study of Riemann problems (i.e. initial value problems whose initial data are scale-invariant). Influence of EOSs on Riemann problems for the Euler equations has been widely discussed in the literature (see the important review article of Menikoff and Plohr [34] and included references). First limited to the perfect gas dynamics system, the theory has been extended to more general EOSs in the 40s by Bethe [5] and Weyl [49]. In addition to thermodynamic consistency, their theory (often referred as the *standard theory*) precisely lies on the additional assumption that the fundamental derivative $\mathscr{G}$ is strictly positive (convex EOSs). Within this context, existence and uniqueness of solutions to Riemann problems were widely discussed in [41]. This additional assumption ($\mathscr{G} > 0$) is generally satisfied by most materials. Nevertheless, it excludes some interesting physical situations. Indeed, near critical points or when phase transitions occur, isentropes usually loose their convexity. Anomalous wave structure then results [8,34,52]: instead of classical (i.e. simple) waves one may encounter composite waves which include split shocks, sonic isentropic compressions or rarefaction shocks (see [19] for a recent review on this topic). As it was reported in [34], loss of convexity leads to non-uniqueness of solutions to Riemann problems which cannot be resolved neither by the standard entropy condition, nor by the Lax criterion [29]. The question of uniqueness is then generally resolved via the Liu-Oleinik criterion [31,32], which is equivalent for all admissible shocks to admit a viscous profile. This was also noticed in Wendroff's work [47,48]. All these properties have been illustrated in [22] where a simplified phase transition EOS has been proposed: on a sample Riemann problem, a continuous family of entropic solutions (i.e. an infinity) has been exhibited, two of them satisfying the Lax criterion, but only one having a viscous profile. This has also an important impact on numerical methods. Since waves must admit viscous profiles, one may expect that numerical schemes require strong enough dissipation to capture the admissible solution. Using a first-order Godunov-type scheme, it was shown in [22] that, parametrized with the Courant number (i.e. depending on the amount of numerical diffusion), this whole family of entropic solutions could be numerically retrieved. This implicitely means that it is the numerical diffusion of the scheme which selects the solution. A legitimate question then concerns the ability of high-order shock capturing schemes to naturally select the physically stable solution.

To investigate this question and evaluate modern as well as future high-order numerical schemes, there is therefore a crucial need for well-documented (realistic) benchmarks. This is precisely the object of this paper. The aim here is to propose a model EOS as simple as possible that mimic the anomalies caused by loss of convexity of isentropes in the (p,τ)-plane and to provide the analytical solution to a complex Riemann problem which covers all these anomalies, namely composite waves.

The model EOS presented in Section 3 has already been proposed in [19–21]. It is a Mie-Grüneisen-type EOS representative of real liquids and solids, but with a quite *bizarre* $\mathscr{C}^\infty$ reference potential for which the sign of the fundamental derivative changes twice: this fictitious material will be called the *Bizarrium* hereafter. Thus its isentropes may smoothly loose their convexity,[1] as it is the case for the van der Waals EOS near a critical point [8,7,34] or for Bethe–Zel'dovich–Thompson (BZT)-fluids [44,9,35]. The present EOS is nevertheless simpler since it naturally satisfies the thermodynamic stability requirements (thus leading to a hyperbolic SCL). Following the precise and complete theoretical analysis given in [19,34], both compressive and expansive branches of the Bizarrium composite wave curves are then briefly described at the end of Section 3. This analysis leads to the benchmark proposal given in Section 4. The constant left and right states of this Riemann test problem have been specially chosen such that the solution consists in a left-facing expansive composite wave (rarefaction/sonic rarefaction shock/rarefaction) and a right-facing compressive composite one (shock/sonic isentropic compression/shock) separated by a contact discontinuity, thus including all the pathologies encountered in such a case.

Due to its simplicity, the Bizarrium EOS can be quickly included in any hydrodynamic code of both Eulerian or Lagrangian type. Along with the reference solution proposed in Section 4, the *Bizarrium test problem* is therefore a quite simple and complete benchmark to evaluate the behavior of numerical schemes on such cases. To illustrate difficulties encountered by various numerical schemes to capture the physical solution, we review in Section 5 two great classes of numerical methods, namely the vNR-type method, introduced in 1950 by von Neumann and Richtmyer [39,46] and the Godunov-type method, introduced in 1959 by Godunov [15]. In the present paper we focus on the Lagrangian approach, but all the numerical schemes reviewed in Section 5 can also be used in Eulerian hydrocodes based on split Lagrange and remapping phases.

The first shock capturing approach recalled in Section 5.1 is based on an internal energy formulation. To achieve second-order accuracy, the historical vNR scheme (Section 5.1.1) is staggered in both space and time. The original vNR scheme is not conservative in total energy, a defect corrected by many variants of the scheme: see for example [2,14,33,38,45,51]. In Section 5.1.2, we recall one of these, namely a version of the BBC scheme reported in the 80s by Woodward and Colella [51]. To deal with shocks, an artificial viscosity q must be added in the momentum and internal energy equations. Various formulations of q, some of them being recalled in Section 5.1.3, are referenced in the literature. Since it seems that depending upon the amount of numerical diffusion the scheme selects a physical or an unphysical solution, a special attention will be paid to its formulation.

The second shock capturing approach recalled in Section 5.2 is based on a total energy formulation and is fully conservative. All unknowns are cell-centered and numerical schemes are based on exact or approximate Riemann solvers. The his-

[1] The important case of *polymorphic phase transformations* (see for instance [52]) may be seen as a limit case of such a smooth non-convex EOS, for which both inflexion points of isentropes are getting closer developing a kink [34].

torical *acoustic* Riemann solver is recalled in Section 5.2.1 but it only leads to a first-order Godunov-type scheme. Hereagain, a special attention will be paid to high-order extensions. Three different approaches that revealed quite robust and successful over the years with general EOSs [25] are then reviewed: the second-order Godunov Anti-Diffusé scheme (GAD) inspired from [11], the arbitrary high-order Godunov Acoustic Invariant Advection one [37] (GAIA) and the second- and third-order Godunov-Hybride one [24] (GoHy). They are respectively described in Sections 5.2.2 to 5.2.3.

Numerical results obtained with all these schemes on the Bizarrium test problem are given in Section 6. For completion, the effective order of the Godunov-type schemes described in Section 5.2 is evaluated on two standard smooth-flow test problems. Results are given in Appendix A.

2. The Lagrangian hydrodynamic equations

Introducing ρ_0 the initial mass density, $\tau = \frac{1}{\rho}$ the specific volume, u the velocity, e the specific total energy and p the pressure, the 1D slab compressible Euler equations in Lagrangian form read

$$\begin{cases} \rho_0 \partial_t \tau - \partial_X u = 0, \\ \rho_0 \partial_t u + \partial_X p = 0, \\ \rho_0 \partial_t e + \partial_X (pu) = 0, \end{cases} \tag{1a}$$

together with the fluid particle trajectories which are solution to

$$\partial_t x = u \text{ with } x_{|t=0} = X. \tag{1b}$$

From mass conservation one also has $\rho_0 dX = \rho dx \overset{\text{def}}{=} dm$, which defines the mass coordinate. Introducing $U = (\tau, u, e)^t$ and $F = (-u, p, pu)^t$, system (1a) and (1b) therefore reads

$$\partial_t U + \partial_m F = 0, \tag{2a}$$

$$\partial_t x = u. \tag{2b}$$

Introducing the specific internal energy $\varepsilon = e - u^2/2$ and manipulating Eq. (1a) one can also replace the last equation (total energy conservation) by $\rho_0 \partial_t \varepsilon + p \partial_X u = 0$ or equivalently by

$$\partial_t \varepsilon + p \partial_t \tau = 0. \tag{3}$$

3. A non-convex equation of state (EOS)

As was said in the introduction section, system (1a) is closed with a complete EOS of the type $\varepsilon = \varepsilon(\tau, S)$ which we discuss now.

3.1. The Mie-Grüneisen formulation

A widely used formulation to modelize solid as well as liquid materials is the Mie-Grüneisen-type EOS. It reduces the function $\varepsilon(\tau, S)$ to corrections about a reference curve only parametrized by τ. Let U_0 denote this reference state (all quantities indexed by 0 will refer to this state hereafter). The (complete) EOS considered here is defined by the following relation

$$\varepsilon(\tau, S) = \varepsilon_{k0}(\tau) + C_{v_0} T_0 \exp\left(\frac{S - S_0}{C_{v_0}} + g(\tau)\right), \tag{4a}$$

where

$$g(\tau) = \Gamma_0 \left(1 - \frac{\tau}{\tau_0}\right). \tag{4b}$$

Here Γ_0 and C_{v_0} are respectively the Grüneisen coefficient and the specific heat at constant volume of the reference state. Both constants are assumed to be strictly positive.

By definition of a complete EOS, all other thermodynamic quantities can be deduced from relations (4a) and (4b). Indeed, the pressure and temperature are deduced from the Gibbs relation:

$$\begin{cases} T(\tau, S) = \dfrac{\partial \varepsilon}{\partial S_{|\tau}} = \dfrac{\varepsilon(\tau, S) - \varepsilon_{k0}(\tau)}{C_{v_0}}, \\ p(\tau, S) = -\dfrac{\partial \varepsilon}{\partial \tau_{|S}} = p_{k0}(\tau) + \frac{\Gamma_0}{\tau_0}(\varepsilon(\tau, S) - \varepsilon_{k0}(\tau)), \end{cases} \tag{5}$$

with

$$p_{k0}(\tau) = -\frac{d\varepsilon_{k0}}{d\tau} = -\varepsilon'_{k0}(\tau). \tag{6}$$

For subsequent developments, we also recall some other thermodynamic quantities and their expression when applied to a Mie-Grüneisen-type EOS (4a) and (4b).

- The adiabatic exponent γ:

$$\gamma \overset{\text{def}}{=} \frac{\tau}{p}\frac{\partial^2 \varepsilon}{\partial \tau^2_{|S}} = -\frac{\tau}{p}\frac{\partial p}{\partial \tau_{|S}} = \frac{\tau}{p}\left(\frac{\Gamma_0}{\tau_0}(p - p_{k0}(\tau)) - p'_{k0}(\tau)\right), \tag{7}$$

from which we deduce the Lagrangian sound speed (ρc):

$$(\rho c)^2 \overset{\text{def}}{=} \frac{\gamma p}{\tau} = \frac{\Gamma_0}{\tau_0}(p - p_{k0}(\tau)) - p'_{k0}(\tau). \tag{8}$$

- The Grüneisen coefficient Γ:

$$\Gamma \overset{\text{def}}{=} -\frac{\tau}{T}\frac{\partial^2 \varepsilon}{\partial S \partial \tau} = \Gamma_0 \frac{\tau}{\tau_0}. \tag{9}$$

- The specific heat at constant volume C_v:

$$C_v \overset{\text{def}}{=} T\left(\frac{\partial^2 \varepsilon}{\partial S^2_{|\tau}}\right)^{-1} = C_{v_0}. \tag{10}$$

- The fundamental derivative $\mathscr{G}$:

$$\mathscr{G} \overset{\text{def}}{=} \frac{1}{2}\frac{\tau^2}{\gamma p}\frac{\partial^2 p}{\partial \tau^2_{|S}} = \frac{1}{2}\frac{\tau^2}{\gamma p}\left(p''_{k0}(\tau) + \left(\frac{\Gamma_0}{\tau_0}\right)^2 (p - p_{k0}(\tau))\right). \tag{11}$$

As was recalled in the introduction section, thermodynamic stability requires that $\varepsilon(\tau, S)$ is a convex function of its arguments (see [3 or 6] for instance). Using (4a) and (4b) and the above definitions, this results in the following inequalities:

$$\begin{cases} \dfrac{\partial^2 \varepsilon}{\partial \tau^2_{|S}} \geqslant 0, \\ \dfrac{\partial^2 \varepsilon}{\partial S^2_{|\tau}} \geqslant 0, \\ \dfrac{\partial^2 \varepsilon}{\partial S^2_{|\tau}}\dfrac{\partial^2 \varepsilon}{\partial \tau^2_{|S}} \geqslant \left(\dfrac{\partial^2 \varepsilon}{\partial S \partial \tau}\right)^2. \end{cases} \iff \begin{cases} (\rho c)^2 \geqslant 0, \\ \frac{T}{C_{v_0}} \geqslant 0, \\ (\rho c)^2 \geqslant C_{v_0}\left(\frac{\Gamma_0}{\tau_0}\right)^2 T. \end{cases} \tag{12}$$

Remark 1. The eigenvalues of system (1a) are real as soon as $(\rho c)^2 \geqslant 0$, so that thermodynamic stability also implies the hyperbolicity of system (1a).

Remark 2. If $(\rho c)^2 \geqslant 0$, the fundamental derivative $\mathscr{G}$ and $\frac{\partial^2 p}{\partial \tau^2_{|S}}$ have the same sign: $\mathscr{G}$ therefore measures the convexity of isentropes in the (p, τ)-plane. In particular, if $\mathscr{G} > 0$, the isentropes are convex.

Assuming that the domain of state space is a region in which $T \geqslant 0$, it can be easily shown, using (5) and (8), that condition (12) reduces to

$$p'_{k0}(\tau) \leqslant 0. \tag{13}$$

Therefore any reference potential $\varepsilon_{k0}(\tau)$ such that (13) holds leads to a thermodynamic consistent EOS.

3.2. The Bizarrium EOS

From what has been described above it is now rather easy to build a thermodynamic consistent EOS whose isentrope in the reference state exhibits two concavity changes: one has just to select an appropriate potential $\varepsilon_{k0}(\tau)$. The fictitious material governed by the following EOS is called the *Bizarrium*.

3.2.1. The Bizarrium EOS definition

For convenience we introduce the variable

$$x = \frac{\tau_0}{\tau} - 1. \tag{14}$$

The complete Bizarrium EOS is given by (4a) and (4b), together with the $\mathscr{C}^\infty$ potential

$$\varepsilon_{k0}(\tau) = \varepsilon_0 - C_{v_0} T_0 (1 + g(\tau)) + \frac{K_0 \tau_0}{2} x^2 F(\tau), \tag{15a}$$

where

$$F(\tau) = f_0(x) = \frac{1 + (\frac{s}{3} - 2)x + qx^2 + rx^3}{1 - sx}, \tag{15b}$$

and the parameters given in Table 1.

From (15b), it is a simple matter to check that

$$\begin{cases} f_1(x) = f_0'(x) = \dfrac{\frac{s}{3} - 2 + 2qx + 3rx^2 + sf_0(x)}{1 - sx}, \\ f_2(x) = f_1'(x) = \dfrac{2q + 6rx + 2sf_1(x)}{1 - sx}, \\ f_3(x) = f_2'(x) = \dfrac{6r + 3sf_2(x)}{1 - sx}. \end{cases} \tag{16}$$

From (6) and (15a) we therefore get

$$\begin{cases} p_{k0}(\tau) = -C_{v_0}T_0\Gamma_0\rho_0 + \frac{K_0x(1+x)^2}{2}[2f_0(x) + xf_1(x)], \\ p_{k0}'(\tau) = -\frac{K_0(1+x)^3\rho_0}{2}[2(1+3x)f_0(x) + 2x(2+3x)f_1(x) + x^2(1+x)f_2(x)], \\ p_{k0}''(\tau) = \frac{K_0(1+x)^4\rho_0^2}{2}[12(1+2x)f_0(x) + 6(1+6x+6x^2)f_1(x) + 6x(1+x)(1+2x)f_2(x) + x^2(1+x)^2f_3(x)], \end{cases} \tag{17}$$

so that all thermodynamic variables defined in the preceding section can now be easily computed.

3.2.2. Domain of validity

The reference potential (15a) is only meaningful for $1 - sx > 0$, which gives a lower bound for the specific volume: τ must be greater than $\frac{s}{1+s}\tau_0$. On the other hand, thermodynamic stability requires that (13) holds. This also gives an upper bound for the specific volume: τ must be smaller than $\alpha\tau_0$, where $\alpha \simeq 1.2325742$. We will therefore assume in the sequel that the specific volume always lies in this interval:

$$l\tau \in \mathscr{D} = \left]\frac{s}{1+s}\tau_0, \alpha\tau_0\right[. \tag{18}$$

This means that for the above EOS to be valid, the Bizarrium density must be comprised between 8113.102 and 16666.666 kg/m^3.

3.3. Anomalous wave structure of the Bizarrium EOS

An analysis of relations (17) shows that $p_{k0}''(\tau) = 0$ for $\tau = 0.875\tau_0$ and $\tau = 0.75\tau_0$, these points being the locus of inflexion of the reference pressure curve $p_{k0}(\tau)$. Since, from (4a) and (5), one has

$$p(\tau, S) = p_{k0}(\tau) + \frac{\Gamma_0}{\tau_0}C_{v_0}T_0\exp\left(\frac{S - S_0}{C_{v_0}} + g(\tau)\right),$$

this leads to two concavity changes for isentropes in the (p, τ)-plane. From Remark 2, the fundamental derivative is therefore negative in a non-empty interval and changes sign twice. As an illustration, p and $\mathscr{G}$ on the isentrope $S = S_0$ are plotted in Fig. 1.

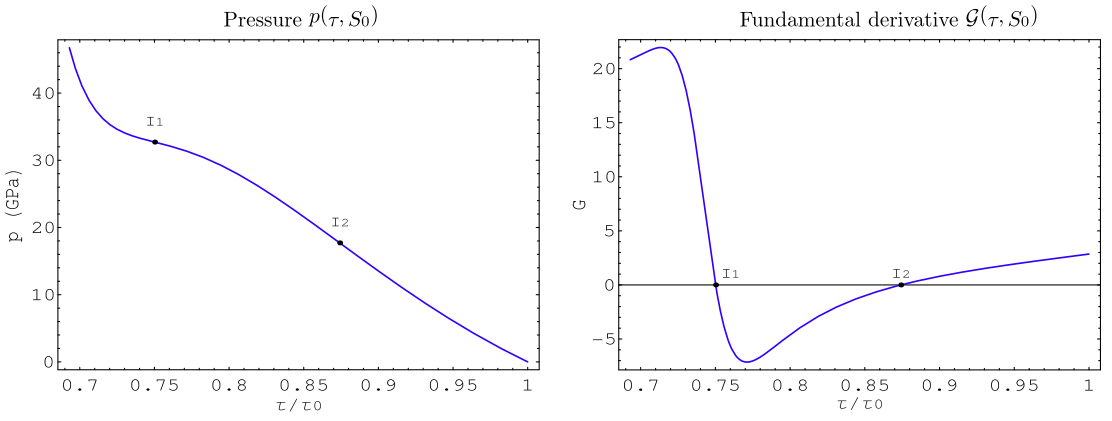

Fig. 1. Bizarrium EOS: pressure and fundamental derivative on the isentrope $S = S_0$, function of the specific volume. I_1 and I_2 are inflexion points of $p(\tau, S_0)$.

When the sign of $\mathscr{G}$ changes, anomalous wave structure results [19,34]. After having briefly recalled general principles to solve Riemann problems, we review the different wave patterns that can be obtained with such an anomalous EOS. For a precise theoretical analysis we refer the reader to [19,34].

3.3.1. Generalities on the Riemann problem for the Euler equations

A Riemann problem (RP) is an initial value problem such that initial conditions are scale-invariant. In one space dimension, initial data therefore consist of two constant states U_l and U_r on both sides of a discontinuity. From the structure of the equations as well as these peculiar initial data, solutions are also expected to be scale-invariant. Since wave curves, by definition, are the locus of all states that can be joined from an initial state U_0 with a scale-invariant solution, solving the RP amounts to construct wave curves associated to U_l and U_r. For the hydrodynamic system (1a), solutions are conceptually easy to build: two families of waves (the 1- and 3-wave) propagates on both sides of a contact discontinuity (the 2-wave), across which only pressure and velocity are continuous. Solving the RP therefore amounts to build wave curves associated to U_l and U_r and to look for their intersection in the (p,u)-plane.

A wave curve associated to an initial state U_0 is composed of two branches: a compressive ($\tau < \tau_0$) and an expansive ($\tau > \tau_0$) part. When the fundamental derivative $\mathscr{G}$ has a constant sign only *simple* waves are allowed [19,34]: smooth isentropic scale-invariant solutions to (1a) or entropic shock waves satisfying the Rankine–Hugoniot jump relations.

For $\mathscr{G} > 0$ – the most common case, also referred as the *standard theory* [5,49] – the compressive part is the locus of all states that can be joined to U_0 by a *compressive* shock wave while the expansive one is the locus of all states that can be joined to U_0 by an isentropic smooth scale-invariant solution to (1a).

Conversely, for $\mathscr{G} < 0$, these results are inverted [19]: the compressive part is the locus of all states that can be joined to U_0 by an isentropic smooth scale-invariant solution to (1a), while the expansive one is the locus of all states that can be joined to U_0 by a *rarefaction* shock wave.

When $\mathscr{G}$ is not of constant sign – as is the case for the Bizarrium EOS – each branch of wave curves are combinations of simple waves which move as a single entity, called *composite* waves. For a simple wave not to approach the other, their propagation speeds must be compatible. As an example, a smooth isentropic wave may be contiguous to a shock wave if and only if it is sonic [19,34,52]. Taking this property into account, wave curves are then built using both particular cases mentioned above, depending upon the sign of $\mathscr{G}$ (see [19]).

The fundamental derivative $\mathscr{G}$ being successively positive/negative/positive in the Bizarrium case, three simple waves may propagate together: the compressive branch consists in a Hugoniot/isentrope/Hugoniot composite curve and conversely, the expansive one in a isentrope/Hugoniot/isentrope composite curve. They are briefly described in the two

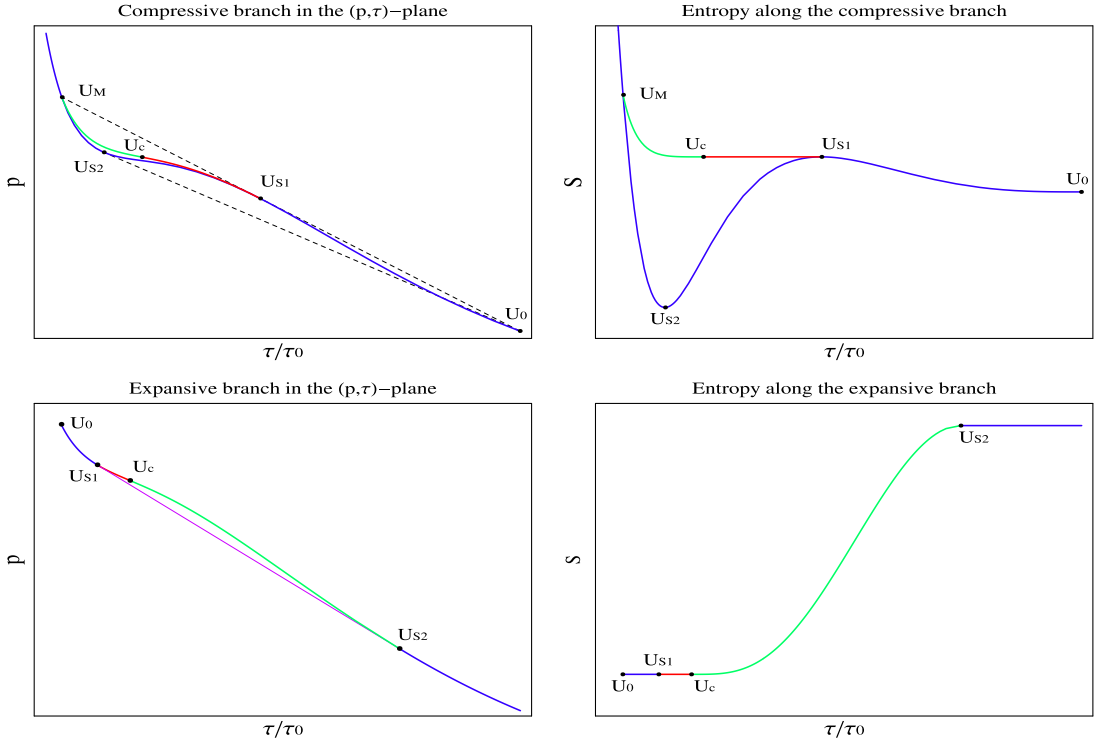

Fig. 2. Bizarrium EOS: anomalous Bizarrium wave curves when crossing a non-convex region. Compressive (top) and expansive (bottom) branches of the composite wave curve in the (p,τ)-plane (left) and entropy along these branches (right).

following paragraphs and for further details we refer the reader to [19,34] for the general theory and to [20,21] for the Bizarrium specific case.

3.3.2. The dynamic compression curve of the Bizarrium

Let us consider the Hugoniot curve $\mathscr{H}_0$ associated to the initial state U_0 (Fig. 2 – top). Such a curve has several noticeable points. There are two sonic points U_{S1} and U_{S2} such that U_{S1} (*resp.* U_{S2}) is a local maximum (*resp.* minimum) of entropy. From [34] we also know that $\mathscr{H}_0$ and isentropes have the same concavity in these points. The fundamental derivative $\mathscr{G}$ is therefore negative in U_{S1}. Following this isentrope for decreasing τ, $\mathscr{G}$ is also negative in a neighbourhood of U_{S1} (by continuity), till the inflexion point U_C. A third noticeable point, denoted U_M, is the point where the Rayleigh line passing through U_{S1} intersects $\mathscr{H}_0$ a second time. Starting from U_0 we get, by increasing the shock strength:

- if $p \leqslant p_{S1}$: a simple classical shock wave. If $p = p_{S1}$, the flow behind the shock wave is sonic.
- If $p_{S1} < p \leqslant p_C$: a sonic shock till state U_{S1}, followed by an isentropic compression wave.
- If $p_C < p < p_M$: a fast shock till state U_{S1}, followed by an isentropic compression wave till a state U_* (such that $p_{S1} < p_* < p_C$), followed by a slow shock. Both ends of the isentropic compression wave are sonic. To each state U_* corresponds a unique final state U given by the intersection of the Hugoniot curve $\mathscr{H}_*$ and the sonic Rayleigh line whose slope is $-(\rho c)_*^2$.
- If $p \geqslant p_M$: a simple classical shock wave.

3.3.3. The dynamic expansion curve of the Bizarrium

Let U_0 be a state such that the isentrope $S_0 = S(U_0)$ passes through the non-convex region for increasing specific volumes (Fig. 2 – bottom). As in the standard case ($\mathscr{G} > 0$), it is possible to build a smooth simple wave along this isentrope till we reach state U_C, such that $\mathscr{G}(U_C) = 0$. It is then not possible to follow S_0 for $\tau > \tau_C$, since wave speeds would not be ordered monotonically: a discontinuity must appear. Hereagain, only one propagation speed is allowed: the state ahead this shock wave must be a sonic state. A noticeable state on S_0, denoted U_{S1} in Fig. 2 (bottom), is the only state such that the Rayleigh line $\mathscr{R}_{S1}$ whose slope is $-(\rho c)_{S1}^2$ is also tangent to $\mathscr{H}_{S1}$ in another state with a lower pressure, namely U_{S2}. Starting from U_0 we get, by decreasing the final pressure:

- if $p \geqslant p_C$: a classical smooth isentropic simple wave.
- If $p_C > p \geqslant p_{S2}$: a smooth isentropic simple wave, till a state U_* such that $p_C < p_* < p_{S1}$ followed by an entropic rarefaction shock, sonic in U_*. To each state U_* corresponds a unique final state U given by the intersection of the Hugoniot curve $\mathscr{H}_*$ and the sonic Rayleigh line whose slope is $-(\rho c)_*^2$. If $p = p_{S2}$, the flow behind the shock wave is also sonic.
- If $p < p_{S2}$: a smooth isentropic simple wave till state U_{S1}, followed by a rarefaction shock till state U_{S2}, followed by another smooth isentropic simple wave. Both ends of the rarefaction shock are sonic.

4. The Bizarrium numerical test problem

The *Bizarrium test problem* defined below has been specially designed to exhibit both complex wave patterns described in the previous section. We also give the semi-analytical solution which has been obtained using a symbolic computation software. The initial condition $U_0(x)$ consists of two constant states on both sides of a discontinuity: $U_0(0 \leqslant x < 0.5) = U_l$ and $U_0(0.5 < x \leqslant 1) = U_r$ with

$$U_l = \begin{cases} \tau_l = 0.7\ 10^{-4}, \\ u_l = 0, \\ p_l = 10^{11}, \end{cases} \quad \text{and} \quad U_r = \begin{cases} \tau_r = 10^{-4}, \\ u_r = 250, \\ p_r = 0. \end{cases}$$

All values are given in the International System of Units. The right state is therefore the reference state whose characteristics are given in Table 1, while the left one is characterized by a specific volume 0.7 times the reference one at a pressure of 100 GPa. Concerning the boundary conditions, easily applied with both Lagrangian and Eulerian hydrocodes, we impose a reflecting wall on the left and a flow-out condition on the right.

Table 1
Coefficients of the Bizarrium EOS.

ρ_0 (kg/m^3)	10,000	s	1.5
K_0 (Pa)	10^{11}		
C_{v_0} (J/kg/K)	1000	q	$-\frac{42080895}{14941154}$
T_0 (K)	300		
ε_0 (J/kg)	0		
S_0	0	r	$\frac{727668333}{149411540}$
Γ_0	1.5		

Analytical composite wave curves associated to these states are plotted in Fig. 3 (top), in the (p,τ) (left) and (p,u) (right) planes. The exact solution to this Riemann problem is the following (states mentioned below are defined in Table 2).

- The left-facing wave is a composite expansive wave consisting in a rarefaction from $U_{y0} = U_l$ to U_{y1}, followed by a rarefaction shock from U_{y1} to U_{y2}, sonic ahead and behind $(D_l = u_{y1} - c_{y1} = u_{y2} - c_{y2})$, followed by a rarefaction from U_{y2} to U_{yz}.
- The right-facing wave is a composite compressive wave consisting in a fast shock from $U_{z0} = U_r$ to U_{z1}, sonic behind $(D_{rf} = u_{z1} + c_{z1})$, followed by an isentropic compression from U_{z1} to U_{z2}, followed by a slow shock from U_{z2} to U_{zy}, sonic ahead $(D_{rs} = u_{z2} + c_{z2})$.
- States U_{yz} and U_{zy} are separated by a contact discontinuity.

The (x,t) diagram and the analytical density profile are given in Fig. 3 (bottom).

Remark 3. Also useful for numerical experiments, two intermediate Riemann problems whose solutions consist in only one composite wave may be extracted from the above *Bizarrium test problem*. Denoting $u^* = 1.31912830324e+03$ the contact discontinuity velocity, these are defined by the following initial and boundary conditions.

Single composite expansive wave

The initial condition is

$$U(x,t=0) = \begin{cases} \tau = 0.7 \times 10^{-4}, \\ u = -u^*, \\ p = 10^{11}, \end{cases}$$

with a flow-out boundary condition imposed on the left and a reflecting wall on the right. The solution is given in Table 2 (top) together with the appropriate Galilean change for material velocity.

Single composite compressive wave

The initial condition is

$$U(x,t=0) = \begin{cases} \tau = 10^{-4}, \\ u = 250 - u^*, \\ p = 0, \end{cases}$$

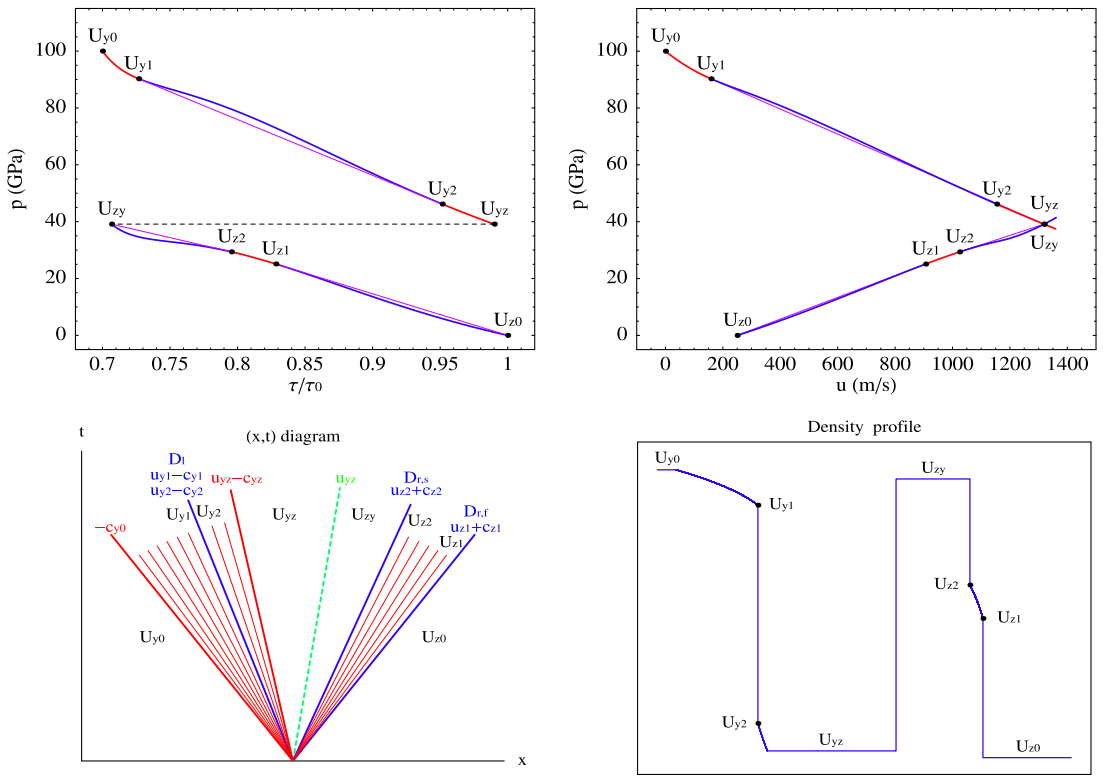

Fig. 3. Solution of the *Bizarrium numerical test problem*. Top: composite wave curves in the (p,τ) (left) and (p,u) (right) planes. Bottom: (x,t) diagram (left) and density profile (right).

Table 2
Bizarrium numerical test problem: reference solution obtained with a symbolic computation code. Values in noticeable points refer to Fig. 3 in SI units: ρ in kg/m^3, p in *Pa*, T in *K*, ε in J/kg, S in J/kg/*K*, c, u and D in m/s.

	Rarefaction $U_{y0} \to U_{y1}$/ Rarefaction shock $U_{y1} \to U_{y2}$/Rarefaction $U_{y2} \to U_{yz}$			
	U_{y0}	U_{y1}	U_{y2}	U_{yz}
Left composite wave				
τ/τ_0	0.7	7.26771712598e−01	9.51530533349e−01	9.90063177596e−01
ρ	1.42857142857e+04	1.37594788386e+04	1.05093842494e+04	1.01003655386e+04
p	1e+11	9.02744810817e+10	4.61924164830e+10	3.91351551833e+10
T	4.34761498896e+03	4.17648443099e+03	3.00982131883e+03	2.84078876598e+03
ε	4.48657821135e+06	4.23449658149e+06	2.70089006334e+06	2.53682071541e+06
S	2.22360022067e+03	2.22360022067e+03	2.23314931883e+03	2.23314931883e+03
c	5.65147161146e+03	3.21862667515e+03	4.21400765023e+03	4.08074131794e+03
u	**0**	1.58878322311e+02	1.15425929739e+03	1.31912830324e+03
D		−3.05974835284e+03		
	Shock $U_{z0} \to U_{z1}$/Isentropic compression $U_{z1} \to U_{z2}$/Shock $U_{z2} \to U_{zy}$			
	U_{zy}	U_{z2}	U_{z1}	U_{z0}
Right composite wave				
τ/τ_0	7.06725240438e−01	7.95477062357e−01	8.28348504127e−01	1
ρ	1.41497705584e+04	1.25710727225e+04	1.20722135070e+04	1.00000000000e+04
p	3.91351551833e+10	2.93828326982e+10	2.51154533425e+10	0
T	4.92847161357e+02	4.22603617534e+02	4.02271608164e+02	3.00000000000e+02
ε	6.09511010352e+05	3.05456197415e+05	2.15555256788e+05	0.
S	5.65044944451e+01	3.58677842099e+01	3.58677842099e+01	0.
c	4.32661332053e+03	2.63689629270e+03	3.16854447133e+03	3.26726185054e+03
u	1.31912830324e+03	1.02492830520e+03	9.06590065091e+02	250
D	3.66182459790e+03		4.07513453642e+03	

with a reflecting wall imposed on the left and a flow-out condition on the right. The solution is given in Table 2 (bottom) together with the appropriate Galilean change for material velocity.

5. A selection of Lagrangian shock capturing schemes

We provide in this section a brief description of various Lagrangian numerical schemes used to compute flows solution to (2a) and (3). Two different approaches, both based on a finite volume method and used for about fifty years now in various hydrocodes, are recalled in Sections 5.1 and 5.2. The main difference between the two approaches is that the first one is based on a non-conservative internal energy formulation, the second being fully conservative, based on a total energy formulation.

The 1D domain $[X_{\min}, X_{\max}]$ is discretized in N cells $I_j = \left[X_{j-\frac{1}{2}}, X_{j+\frac{1}{2}}\right]$, with $X_{\frac{1}{2}} = X_{\min}$ and $X_{N+\frac{1}{2}} = X_{\max}$. The mass coordinates are therefore given by

$$\begin{cases} m_{\frac{1}{2}} = 0, \\ m_{j+\frac{1}{2}} = m_{j-\frac{1}{2}} + \Delta m_j \text{ for } j = 2, \ldots, N, \end{cases} \text{with } \Delta m_j = \int_{X_{j-\frac{1}{2}}}^{X_{j+\frac{1}{2}}} \rho_0 dx = \rho_{0,j} \Delta X_j.$$

5.1. vNR-type schemes

With this class of schemes initiated by von Neumann and Richtmyer in 1950 [39,46], the unknowns are cell-centered, except the velocity which is defined at each mesh interface. The historical vNR scheme, which is also staggered in time, is recalled in Section 5.1.1. The BBC variant of this scheme, reported in the 80s by Woodward and Colella in [51] uses velocities defined at each node (staggered in space), but is unstaggered in time (see Section 5.1.2). With both variants, to deal with shocks, an artificial viscosity q must be added in the momentum and internal energy equations. Various formulations of q can be found in the literature. Some of them will be recalled in Section 5.1.3.

5.1.1. The vNR scheme

The discretized equations are the continuity equation ($\rho^0 dX = \rho dx$) and

$$\partial_t u + \partial_m \pi = 0,$$
$$\partial_t \varepsilon + \pi \partial_t \tau = 0,$$

with $\pi = p + q$, q being an artificial viscosity term, usually defined by (see [4] for instance)

$$q = \begin{cases} -c_q \rho \Delta u |\Delta u| - c_l \rho c \Delta u & \text{if } \Delta u < 0, \\ 0 & \text{otherwise}, \end{cases}$$

where c_q and c_l denote respectively quadratic and linear artificial viscosity coefficients.

To achieve second-order accuracy, all finite differences are centered. The velocity is defined here at each node of the mesh $x_{j+\frac{1}{2}}$ and is also staggered in time (*i.e.* defined at $t^{n+\frac{1}{2}}$). We refer the reader to [46,39] for further details.

The nodal mass being defined by (30), the algorithm consists in solving successively

1. Computation of the velocity and node positions at time $t^{n+\frac{1}{2}}$:

$$u_{j+\frac{1}{2}}^{n+\frac{1}{2}} = u_{j+\frac{1}{2}}^{n-\frac{1}{2}} - \frac{\Delta t}{\Delta m_{j+\frac{1}{2}}} \left(\left(p_{j+1}^n + q_{j+1}^{n-\frac{1}{2}} \right) - \left(p_j^n + q_j^{n-\frac{1}{2}} \right) \right),$$

$$x_{j+\frac{1}{2}}^{n+1} = x_{j+\frac{1}{2}}^n + \Delta t u_{j+\frac{1}{2}}^{n+\frac{1}{2}},$$

2. Computation of the density (and specific volume) at time t^{n+1}:

$$\rho_j^{n+1} = \frac{1}{\tau_j^{n+1}} = \frac{\Delta m_j}{x_{j+\frac{1}{2}}^{n+1} - x_{j-\frac{1}{2}}^{n+1}},$$

3. Approximation of the artificial viscosity at time $t^{n+\frac{1}{2}}$:

$$\tilde{q}_j^{n+\frac{1}{2}} = \begin{cases} -\frac{2c_q}{\tau_j^{n+1} + \tau_j^n} \Delta u_j |\Delta u_j| - c_l (\rho c)_j^n \Delta u_j & \text{if } \Delta u_j = u_{j+\frac{1}{2}}^{n+\frac{1}{2}} - u_{j-\frac{1}{2}}^{n+\frac{1}{2}} < 0, \\ 0 & \text{otherwise}, \end{cases}$$

4. Computation of the internal energy at time t^{n+1}:

$$\varepsilon_j^{n+1} = \varepsilon_j^n - \left(\frac{1}{2} (p_j^{n+1} + p_j^n) + \tilde{q}_j^{n+\frac{1}{2}} \right) (\tau_j^{n+1} - \tau_j^n),$$

5. Computation of the artificial viscosity at time $t^{n+\frac{1}{2}}$:

$$q_j^{n+\frac{1}{2}} = \begin{cases} -c_q \rho_j^{n+1} \Delta u_j |\Delta u_j| - c_l (\rho c)_j^{n+1} \Delta u_j & \text{if } \Delta u_j = u_{j+\frac{1}{2}}^{n+\frac{1}{2}} - u_{j-\frac{1}{2}}^{n+\frac{1}{2}} < 0, \\ 0 & \text{otherwise}. \end{cases}$$

The stability criterion is

$$\begin{cases} \max\limits_j \left(\frac{(\rho c)_j^n}{\Delta m_j}, \frac{|\rho_j^n - \rho_j^{n-1}|}{\rho_j^n \Delta t^n} \right) \Delta t^{n+1} < 1, \\ \Delta t = \min \left(\Delta t^{n+1}, \frac{1}{2} (\Delta t^n + \Delta t^{n+1}) \right). \end{cases}$$

5.1.2. The unstaggered in time BBC scheme

This scheme reported in [51] is recalled here with a different choice of artificial viscosity. Velocities are still defined at each node of the mesh, but in contrast to the vNR scheme, they are defined at time t^n like other quantities: the BBC scheme is staggered in space but unstaggered in time. To achieve second-order accuracy in time, two intermediate levels in time, denoted hereafter $t^{n+\frac{1}{4}}$ and $t^{n+\frac{1}{2}}$ are necessary. Here again, the scheme is formulated in internal energy and artificial viscosity must be added to deal with shocks. It is to be noticed that since all quantities are defined at the same time, there is no ambiguity to define the total energy. Although formulated in internal energy, this scheme is conservative in total energy. With notations introduced in the previous section, the discretized equations are

$$\partial_t \tau - \partial_m u = 0,$$
$$\partial_t u + \partial_m \pi = 0,$$
$$\partial_t \varepsilon + \pi \partial_t \tau = 0.$$

At time t^n, the density (or the specific volume), the velocity and the total energy are known. A time step consists of the following algorithm:

1. Computation of the artificial viscosity and first prediction of the velocity at time $t^{n+\frac{1}{4}}$:

$$q_j^n = \begin{cases} -c_q \rho_j^n \Delta u_j |\Delta u_j| - c_l (\rho c)_j^n \Delta u_j & \text{if } \Delta u_j = u_{j+\frac{1}{2}}^n - u_{j-\frac{1}{2}}^n < 0, \\ 0 & \text{otherwise}, \end{cases}$$

$$u_{j+\frac{1}{2}}^{n+\frac{1}{4}} = u_{j+\frac{1}{2}}^n - \frac{\Delta t}{4} \frac{((p_{j+1}^n + q_{j+1}^n) - (p_j^n + q_j^n))}{\Delta m_{j+\frac{1}{2}}}.$$

2. Prediction at time $t^{n+\frac{1}{2}}$:

$$\left.\begin{aligned}\tau_j^{n+\frac{1}{2}} &= \tau_j^n + \tfrac{1}{2}\tfrac{\Delta t}{\Delta m_j}\left(u_{j+\frac{1}{2}}^{n+\frac{1}{4}} - u_{j-\frac{1}{2}}^{n+\frac{1}{4}}\right)\\ \varepsilon_j^{n+\frac{1}{2}} &= \varepsilon_j^n - (p_j^n + q_j^n)\left(\tau_j^{n+\frac{1}{2}} - \tau_j^n\right)\end{aligned}\right\} \Rightarrow p_j^{n+\frac{1}{2}} = p\left(\tau_j^{n+\frac{1}{2}}, \varepsilon_j^{n+\frac{1}{2}}\right).$$

$$u_{j+\frac{1}{2}}^{n+\frac{1}{2}} = u_{j+\frac{1}{2}}^n - \frac{\Delta t}{2}\frac{\left(\left(p_{j+1}^{n+\frac{1}{2}} + q_{j+1}^n\right) - \left(p_j^{n+\frac{1}{2}} + q_j^n\right)\right)}{\Delta m_{j+\frac{1}{2}}}.$$

3. Finalization at time t^{n+1}:

$$\left.\begin{aligned}x_{j+\frac{1}{2}}^{n+1} &= x_{j+\frac{1}{2}}^n + \Delta t u_{j+\frac{1}{2}}^{n+\frac{1}{2}},\\ u_{j+\frac{1}{2}}^{n+1} &= 2u_{j+\frac{1}{2}}^{n+\frac{1}{2}} - u_{j+\frac{1}{2}}^n,\\ \tau_j^{n+1} &= \tau_j^n + \tfrac{\Delta t}{\Delta m_j}\left(u_{j+\frac{1}{2}}^{n+\frac{1}{2}} - u_{j-\frac{1}{2}}^{n+\frac{1}{2}}\right)\\ \varepsilon_j^{n+1} &= \varepsilon_j^n - \left(p_j^{n+\frac{1}{2}} + q_j^n\right)(\tau_j^{n+1} - \tau_j^n)\end{aligned}\right\} \Rightarrow p_j^{n+1} = p(\tau_j^{n+1}, \varepsilon_j^{n+1}).$$

If needed, the total energy is defined by

$$e_j^{n+1} = \varepsilon_j^{n+1} + \frac{1}{8}\left(\frac{\Delta m_{j-1} + \Delta m_j}{\Delta m_j}\left(u_{j-\frac{1}{2}}^{n+1}\right)^2 + \frac{\Delta m_j + \Delta m_{j+1}}{\Delta m_j}\left(u_{j+\frac{1}{2}}^{n+1}\right)^2\right). \tag{19}$$

The stability criterion is given by the standard CFL condition

$$\max_j(\rho c)_j \frac{\Delta t}{\Delta m_j} \leqslant 1. \tag{20}$$

5.1.3. Artificial viscosity formulations

In Section 5.1 we have given the expression of the artificial viscosity q as it is usually described (see [4] for instance). Many expressions of q have been used since the historical paper of von Neumann and Richtmyer [46]. They are generally written as the sum of a linear and a quadratic term in Δu. The latter term concentrates the artificial viscosity near the shock front while the former one has a more diffuse effect. Some of them are listed below.

- von Neumann–Richtmyer q [46]:

$$q = -c_q\rho\Delta u|\Delta u|. \tag{21}$$

- Rosenbluth q [30,39]:

$$q = \begin{cases} -c_q\rho\Delta u|\Delta u| & \text{if } \Delta u < 0,\\ 0 & \text{otherwise.}\end{cases} \tag{22}$$

- Landshoff q [28]:

$$q = \begin{cases} -c_q\rho\Delta u|\Delta u| - c_l\rho c\Delta u & \text{if } \Delta u < 0,\\ 0 & \text{otherwise.}\end{cases} \tag{23}$$

- "Magical" q combination[2]:

$$q = \begin{cases} -c_q\rho\Delta u|\Delta u| - c_l\rho c\Delta u & \text{if } \Delta u < 0,\\ -c_l\rho c\Delta u & \text{otherwise.}\end{cases} \tag{24}$$

To increase accuracy in the computation of the artificial viscosity and following Christensen [4], one often uses an affine approximation of the velocity in each cell. Let us denote $\Delta u_j^{(1)} = u_{j+\frac{1}{2}} - u_{j-\frac{1}{2}}$ the jump of velocity in cell j. A second-order approximation of this jump is

$$\begin{aligned}\Delta u_j^{(2)} &= \Delta u_j^{(1)} - \frac{1}{2}\Delta m_j\left(\left(\frac{\partial u}{\partial m}\right)_{j+\frac{1}{2}} + \left(\frac{\partial u}{\partial m}\right)_{j-\frac{1}{2}}\right),\\ &= \Delta u_j^{(1)}\left(1 - \frac{1}{2}\left(\left(\frac{\partial u}{\partial m}\right)_{j+\frac{1}{2}}\Big/\left(\frac{\partial u}{\partial m}\right)_j + \left(\frac{\partial u}{\partial m}\right)_{j-\frac{1}{2}}\Big/\left(\frac{\partial u}{\partial m}\right)_j\right)\right),\\ &= \Delta u_j^{(1)}\left(1 - \frac{1}{2}(\varphi_j^+ + \varphi_j^-)\right),\end{aligned}$$

[2] To our knowledge, the "Magical" q formulation combining features of the vNR, Rosenbluth and Landshoff artificial viscosities is not referenced in the literature.

where

$$\left(\frac{\partial u}{\partial m}\right)_j = \frac{\Delta u_j^{(1)}}{\Delta m_j} \quad \text{and} \quad \varphi_j^{\pm} = \left(\frac{\partial u}{\partial m}\right)_{j\pm\frac{1}{2}} \Big/ \left(\frac{\partial u}{\partial m}\right)_j.$$

To preserve monotonicity, limiters have to be used. Introducing

$$r_j^{\pm} = \left(\frac{\Delta u_{j\pm1}^{(1)}}{\Delta m_{j\pm1}}\right) \Big/ \left(\frac{\Delta u_j^{(1)}}{\Delta m_j}\right),$$

three different ones will be considered:

$$\varphi_j^{\pm} = \max(0, \min(1, r_j^{\pm})), \text{the Minmod limiter}, \tag{25a}$$

$$\varphi_j^{\pm} = \max(0, \min(1, 2r_j^{\pm}), \min(2, r_j^{\pm})), \text{the Superbee limiter}, \tag{25b}$$

$$\varphi_j^{\pm} = \max\left(0, \min\left(2, 2r_j^{\pm}, \frac{\Delta m_j r_j^{\pm} + \Delta m_{j\pm1}}{\Delta m_j + \Delta m_{j\pm1}}\right)\right), \text{ the Christensen limiter}. \tag{25c}$$

5.2. Godunov-type schemes

In contrast to vNR-type schemes, the class of schemes introduced by Godunov in 1959 [15] is based on a total energy formulation and all unknowns are cell-centered. Given a mesh size Δm_j, an approximation U_j^n of $U(m_j, t^n)$ at time t^n is defined by

$$U_j^n = \frac{1}{\Delta m_j} \int_{m_{j-\frac{1}{2}}}^{m_{j+\frac{1}{2}}} U(m, t^n) dm. \tag{26}$$

Introducing the time step $\Delta t = t^{n+1} - t^n$, an explicit Lagrangian Godunov-type scheme reads

$$U_j^{n+1} = U_j^n - \frac{\Delta t}{\Delta m_j}\left(F(U)_{j+\frac{1}{2}}^n - F(U)_{j-\frac{1}{2}}^n\right), \tag{27}$$

where $F(U)_{j+\frac{1}{2}}^n = (-u^*, p^*, (pu)^*)_{j+\frac{1}{2}}^t$ is the numerical flux. Solving (2a–b) with a Godunov-type scheme therefore amounts to define these fluxes. This is done via exact or approximate Riemann solvers. Note that having determined $u_{j+\frac{1}{2}}^*$ and $p_{j+\frac{1}{2}}^*$ the last component of the flux is classically defined by $(pu)_{j+\frac{1}{2}}^* = p_{j+\frac{1}{2}}^* u_{j+\frac{1}{2}}^*$. Otherwise stated, this is the choice we made in the following.

We recall in Section 5.2.1 the historical acoustic Riemann solver. This solver leads only to a first-order accurate Godunov-type scheme. To increase the order of accuracy, three different approaches used in the hydrocode platform HERA [25] and described in Sections 5.2.2–5.2.4 are then reviewed.

5.2.1. The (historical) first-order acoustic Riemann solver

To build this approximate Riemann solver, a classical way to proceed is to use the linearized Riemann invariants. Indeed, along the characteristic curves $C_{\pm}$ defined by $dm = \pm(\rho c)dt$, we have $dp \pm (\rho c)du = 0$ so that integration on these curves leads to

$$\begin{cases} \left(p_{j+\frac{1}{2}}^* - p_j\right) + (\rho c)_j\left(u_{j+\frac{1}{2}}^* - u_j\right) = 0 & \text{along } C^+ \text{coming from the cell } I_j, \\ \left(p_{j+\frac{1}{2}}^* - p_{j+1}\right) - (\rho c)_{j+1}\left(u_{j+\frac{1}{2}}^* - u_{j+1}\right) = 0 & \text{along } C^- \text{coming from the cell } I_{j+1}. \end{cases}$$

This 2×2 linear system can be easily solved. It yields to

$$\begin{cases} p_{j+\frac{1}{2}}^{*,O1} = \dfrac{(\rho c)_j p_{j+1} + (\rho c)_{j+1} p_j}{(\rho c)_j + (\rho c)_{j+1}} + \dfrac{(\rho c)_j (\rho c)_{j+1}}{(\rho c)_j + (\rho c)_{j+1}}(u_j - u_{j+1}), \\ u_{j+\frac{1}{2}}^{*,O1} = \dfrac{(\rho c)_j u_j + (\rho c)_{j+1} u_{j+1}}{(\rho c)_j + (\rho c)_{j+1}} + \dfrac{1}{(\rho c)_j + (\rho c)_{j+1}}(p_j - p_{j+1}), \end{cases} \tag{28}$$

which is the well-known acoustic Riemann solver[3]. It is proved in [12] that the Godunov scheme together with the acoustic Riemann solver (28) is entropic under the CFL condition (20). Having defined the velocities of interfaces, Eq. (2b) is discretized in the following way

[3] Formulae (28) are given in Godunov's seminal paper [15], to justify an optimal Lagrangian mesh criteria on material interfaces. A simpler acoustic solver setting $(\rho c)_j = (\rho c)_{j+1}$ is also detailed for the p-system with a numerical result, a work that played a key role in the derivation of the general nonlinear method [16]. Very curiously, the *acoustic* Riemann solver is then disregarded for the Euler equations in Lagrangian coordinates, the iterative *exact* Riemann solver being considered instead, in the perfect gas case. In subsequent works [1,18,17], the Lagrangian formulation will not be mentioned any more, with *unsplit* Eulerian or "moving grid" numerical fluxes that cannot be treated in the acoustic approximation.

$$x_{j+\frac{1}{2}}^{n+1} = x_{j+\frac{1}{2}}^{n} + \Delta t u_{j+\frac{1}{2}}^{*}. \tag{29}$$

The scheme (27) together with the Riemann solver (28) is only first-order accurate. Next we briefly recall high-order extensions of this scheme (in both space and time), focusing on methods that can be developed to any order of accuracy.

5.2.2. The GAD numerical fluxes (for Godunov Anti-Diffusé)

To limit diffusion of the acoustic Riemann solver (28) one can add to it an anti-diffusive term. Since this latter generates spurious oscillations near discontinuities, the anti-diffusive term has to be limited [11]. Let $u_{j+\frac{1}{2}}^{*,O1}$ and $p_{j+\frac{1}{2}}^{*,O1}$ denote the solutions of the Riemann problem at interface $x_{j+\frac{1}{2}}$ obtained with the acoustic Riemann solver (28). Let also introduce

$$v_{j+\frac{1}{2}} = \frac{(\rho c)_j + (\rho c)_{j+1}}{2} \frac{\Delta t}{\Delta m_{j+\frac{1}{2}}},$$

where $\Delta m_{j+\frac{1}{2}}$ is the nodal mass given by

$$\Delta m_{j+\frac{1}{2}} = \frac{1}{2}(\Delta m_j + \Delta m_{j+1}). \tag{30}$$

The GAD numerical fluxes write the following way[4]:

$$\begin{cases} u_{j+\frac{1}{2}}^{*,GAD} = u_{j+\frac{1}{2}}^{*,O1} + \frac{1}{2}\left(1 - v_{j+\frac{1}{2}}\right)\left[\varphi_{j+\frac{1}{2}}^{u,+}\left(u_{j+1} - u_{j+\frac{1}{2}}^{*,O1}\right) - \varphi_{j+\frac{1}{2}}^{u,-}\left(u_{j+\frac{1}{2}}^{*,O1} - u_j\right)\right], \\ p_{j+\frac{1}{2}}^{*,GAD} = p_{j+\frac{1}{2}}^{*,O1} + \frac{1}{2}\left(1 - v_{j+\frac{1}{2}}\right)\left[\varphi_{j+\frac{1}{2}}^{p,+}\left(p_{j+1} - p_{j+\frac{1}{2}}^{*,O1}\right) - \varphi_{j+\frac{1}{2}}^{p,-}\left(p_{j+\frac{1}{2}}^{*,O1} - p_j\right)\right], \end{cases} \tag{31}$$

where $\varphi_{j+\frac{1}{2}}^{\alpha,\pm}$ for $\alpha = u$ or p is the limiter we discuss now. To that end we introduce

$$r_{j+\frac{1}{2}}^{\alpha,-} = \frac{\alpha_{j+\frac{3}{2}}^{*} - \alpha_{j+1}}{\alpha_{j+\frac{1}{2}}^{*} - \alpha_j} \quad \text{and} \quad r_{j+\frac{1}{2}}^{\alpha,+} = \frac{\alpha_j - \alpha_{j-\frac{1}{2}}^{*}}{\alpha_{j+1} - \alpha_{j+\frac{1}{2}}^{*}},$$

and define

$$\varphi_{j+\frac{1}{2}}^{\alpha,\pm} = \varphi\left(r_{j+\frac{1}{2}}^{\alpha,\pm}\right).$$

Various limiters can therefore be defined. In the following sections, we will use

$$\varphi(r) = \max(0, \min(1, r)), \text{the Minmod limiter}, \tag{32a}$$

$$\varphi(r) = \max(0, \min(1, 2r), \min(2, r)), \text{the Superbee limiter}. \tag{32b}$$

5.2.3. The GAIA numerical fluxes (for Godunov Acoustic Invariant Advection)

Arbitrary high-order schemes for the linear advection equation have been considered in [37] and applied to the linear wave equation. Such schemes, based on a recursive formula for the advection flux, have also been used in the above paper for a high-order generalization of the Godunov method in the case of the locally linearized Euler equations. Strictly speaking, these schemes are of the prescribed high-order accuracy (in both space and time) only in the linear wave limit of the Euler equations in Lagrangian coordinates[5]. The idea is to apply the advection flux recursive formula to the two decoupled advection equations satisfied by the Riemann invariants $J^{\pm} = u \pm \int (\rho c)^{-1} dp$, namely $\partial_t J^{\pm} \pm (\rho c)\partial_m J^{\pm} = 0$ [40]. Without going further into the details, we now briefly describe this scheme.

Let us define the linearized Riemann invariants $J_j^{\pm,n} = u_j^n \pm (\rho c)_j^{-1} p_j^n$ and $\widetilde{J}_{j,k}^{\pm,n} = u_k^n \pm (\rho c)_j^{-1} p_k^n$. Using the recursive formulae (33) it is possible to compute $J_{j+\frac{1}{2}}^{\pm}$ at a prescribed order N in both space and time:

$$\begin{cases} J_{j+\frac{1}{2}}^{+,N} = J_{j+\frac{1}{2}}^{+,N-1} - \frac{1}{N!}\left(\prod_{\substack{i=-m \\ i\neq 0}}^{M} (v_j^+ + i)\right)\left(\sum_{k=0}^{N-1} (-1)^{k+N} C_{N-1}^{k} \widetilde{J}_{j\,j+m-k}^{+,n}\right), \\ J_{j+\frac{1}{2}}^{-,N} = J_{j+\frac{1}{2}}^{-,N-1} - \frac{1}{N!}\left(\prod_{\substack{i=-M \\ i\neq 0}}^{m} (v_{j+1}^- + i)\right)\left(\sum_{k=0}^{N-1} (-1)^{k+N} C_{N-1}^{k} \widetilde{J}_{j+1\,j+M-k+1}^{-,n}\right), \end{cases} \tag{33}$$

with $v_j^{\pm} = \pm(\rho c)_j \frac{\Delta t}{\Delta m_j}$, $m = E\left(\frac{N}{2}\right)$, $M = E\left(\frac{N-1}{2}\right)$ and $C_n^p = \frac{n!}{p!(n-p)!}$. These recursive formulae are initialized with the upwind values of $J^{\pm}$ at the interface $x_{j+\frac{1}{2}}$, *i.e.* $J_{j+\frac{1}{2}}^{+,1} = J_j^{+,n}$ and $J_{j+\frac{1}{2}}^{-,1} = J_{j+1}^{-,n}$, corresponding to the first-order *acoustic* Riemann solver (28).

[4] The original GAD flux of Desgraz [11] in the mid 80s used Dukovicz's Riemann solver [13] for the 1st-order term, with *ad hoc* per-material *EOS-fitted* coefficients, instead of the *acoustic* solver considered here that is coefficient-free.

[5] These schemes are also of the prescribed high-order accuracy in the linear advection limit of the Euler equations in Eulerian coordinates, when used with a Lagrange + high-order remapping approach.

To prevent numerical oscillations near shocks, these high-order Riemann invariants are connected to the first-order ones (see paragraph 5.2.1) via a limiter φ. Defining

$$\begin{cases} r^+_{j+\frac12} = \left(\frac{\widetilde{J}^{+,n}_{jj} - \widetilde{J}^{+,n}_{jj-1}}{\Delta m_{j-\frac12}}\right) \Big/ \left(\frac{\widetilde{J}^{+,n}_{jj+1} - \widetilde{J}^{+,n}_{jj}}{\Delta m_{j+\frac12}}\right), \\ r^-_{j+\frac12} = \left(\frac{\widetilde{J}^{-,n}_{j+1j+2} - \widetilde{J}^{-,n}_{j+1j+1}}{\Delta m_{j+\frac12}}\right) \Big/ \left(\frac{\widetilde{J}^{-,n}_{j+1j+1} - \widetilde{J}^{-,n}_{j+1j}}{\Delta m_{j+\frac12}}\right), \end{cases} \quad \text{and} \quad \varphi^\pm_{j+\frac12} = \varphi\left(r^\pm_{j+\frac12}\right),$$

where $\Delta m_{j+\frac12}$ is given by (30), the limited high-order Riemann invariants read

$$J^{\pm,lim}_{j+\frac12} = J^{\pm,1}_{j+\frac12} + \varphi^\pm_{j+\frac12}\left(J^{\pm,N}_{j+\frac12} - J^{\pm,1}_{j+\frac12}\right).$$

Corresponding high-order values of $u^{*,lim}_{j+\frac12}$ and $p^{*,lim}_{j+\frac12}$ are then obtained by solving the linear system

$$\begin{cases} J^{+,lim}_{j+\frac12} = u^{*,lim}_{j+\frac12} + (\rho c)^{-1}_j p^{*,lim}_{j+\frac12}, \\ J^{-,lim}_{j+\frac12} = u^{*,lim}_{j+\frac12} - (\rho c)^{-1}_{j+1} p^{*,lim}_{j+\frac12}. \end{cases} \tag{34}$$

Various limiters can be used. In the sequel we will choose the Minmod limiter (32a). Two other limiting techniques inspired from [10,37,42] will also be used and are recalled below.

The TVD limiter

Denoting $[\![\alpha_1, \ldots, \alpha_p]\!] = [\min(\alpha_1, \ldots, \alpha_p), \max(\alpha_1, \ldots, \alpha_p)]$, building a TVD flux amounts to enforce

$$\begin{cases} J^{+,TVD}_{j+\frac12} \in [\![\widetilde{J}^{+,n}_{jj}, \widetilde{J}^{+,n}_{jj+1}]\!] \cap [\![\widetilde{J}^{+,n}_{jj}, J^{+,UL}_j]\!], \\ J^{-,TVD}_{j+\frac12} \in [\![\widetilde{J}^{-,n}_{j+1j}, \widetilde{J}^{-,n}_{j+1j+1}]\!] \cap [\![\widetilde{J}^{-,n}_{j+1j+1}, J^{-,UL}_{j+1}]\!], \end{cases} \tag{35a}$$

where

$$\begin{cases} J^{+,UL}_j = \widetilde{J}^{+,n}_{jj} + \frac{1-v^+_j}{v^+_j}\left(\widetilde{J}^{+,n}_{jj} - \widetilde{J}^{+,n}_{jj-1}\right), \\ J^{-,UL}_j = \widetilde{J}^{-,n}_{jj} - \frac{1+v^-_j}{v^-_j}\left(\widetilde{J}^{-,n}_{jj} - \widetilde{J}^{-,n}_{jj+1}\right). \end{cases} \tag{35b}$$

The MP limiter (*for Monotonicity Preserving*)

Defining

$$\begin{cases} \alpha^{\pm,n}_{j,k} = \widetilde{J}^{\pm,n}_{j,k-1} - 2\widetilde{J}^{\pm,n}_{j,k} + \widetilde{J}^{\pm,n}_{j,k+1}, \\ \alpha^{\pm,n}_{j,k+\frac12} = \text{minmod}(4\alpha^{\pm,n}_{j,k} - \alpha^{\pm,n}_{j,k+1}, 4\alpha^{\pm,n}_{j,k+1} - \alpha^{\pm,n}_{j,k}, \alpha^{\pm,n}_{j,k}, \alpha^{\pm,n}_{j,k+1}), \end{cases}$$

the MP limiter consists in enforcing

$$\begin{cases} J^{+,MP}_{j+\frac12} \in [\![\widetilde{J}^{+,n}_{jj}, \widetilde{J}^{+,n}_{jj+1}, J^{+,MD}_{j+\frac12}]\!] \cap [\![\widetilde{J}^{+,n}_{jj}, J^{+,UL}_j, J^{+,LC}_j]\!], \\ J^{-,MP}_{j+\frac12} \in [\![\widetilde{J}^{-,n}_{j+1j}, \widetilde{J}^{-,n}_{j+1j+1}, J^{-,MD}_{j+\frac12}]\!] \cap [\![\widetilde{J}^{-,n}_{j+1j+1}, J^{-,UL}_{j+1}, J^{-,LC}_{j+1}]\!], \end{cases} \tag{36a}$$

where

$$\begin{cases} J^{+,MD}_{j+\frac12} = \frac12\left(\widetilde{J}^{+,n}_{jj} + \widetilde{J}^{+,n}_{jj+1} - \alpha^{+,n}_{jj+\frac12}\right), \\ J^{-,MD}_{j+\frac12} = \frac12\left(\widetilde{J}^{-,n}_{j+1j} + \widetilde{J}^{-,n}_{j+1j+1} - \alpha^{-,n}_{j+1j+\frac12}\right), \\ J^{+,LC}_j = \widetilde{J}^{+,n}_{jj} + \frac{1-v^+_j}{2v^+_j}\left(\widetilde{J}^{+,n}_{jj} - \widetilde{J}^{+,n}_{jj-1} + \alpha^{+,n}_{jj-\frac12}\right), \\ J^{-,LC}_j = \widetilde{J}^{-,n}_{jj} - \frac{1+v^-_j}{2v^-_j}\left(\widetilde{J}^{-,n}_{jj} - \widetilde{J}^{-,n}_{jj+1} + \alpha^{-,n}_{jj+\frac12}\right). \end{cases} \tag{36b}$$

Note that the MP-limited interface values $J^{\pm,lim}_{j+\frac12}$ lie in larger intervals than the TVD-ones (35a).

5.2.4. The GoHy numerical fluxes (for Godunov-Hybride)

At interface x_0, the exact numerical flux between t^n and t^{n+1}, which is given by

$$\varphi^* = \frac{1}{\Delta t}\int_{t^n}^{t^{n+1}} \varphi(x_0, t)dt, \text{ for } \varphi = (-u, p, pu)^t,$$

can be approximated by

$$\varphi^* = \frac{1}{\Delta t}\int_{t^n}^{t^{n+1}} \left(\varphi_0^n + \left(\frac{\partial\varphi}{\partial t}\right)_0^n (\theta - t^n) + \frac{1}{2}\left(\frac{\partial^2\varphi}{\partial t^2}\right)_0^n (\theta - t^n)^2 + \cdots\right) d\theta,$$
$$= \varphi_0^n + \frac{1}{2}\Delta t\left(\frac{\partial\varphi_0}{\partial t}\right)^n + \frac{1}{6}\Delta t^2\left(\frac{\partial^2\varphi_0}{\partial t^2}\right)^n + \cdots.$$

The procedure is to compute this integral at the desired order, replacing temporal derivatives by spatial ones. Indeed, the impulse and total energy equations can be manipulated to give

$$\begin{cases} \partial_t u = -\partial_m p, \\ \partial_t p = -(\rho c)^2 \partial_m u. \end{cases} \tag{37}$$

From (11) one also gets after few manipulations $\frac{\partial(\rho c)}{\partial\tau}_{|S} = -\rho^2 c\mathscr{G}$. We therefore have

$$\partial_t(\rho c)^2 = -2\rho(\rho c)^2\mathscr{G}\partial_m u. \tag{38}$$

Let u_0, p_0 and $(pu)_0$ denote approximations of u, p and pu at interface x_0. Using (37), (38) and subsequent derivations (Cauchy–Kovaleskaya procedure), we therefore get

$$\begin{cases} u^* = u_0^n - \frac{\Delta t}{2}\partial_m p + \frac{\Delta t^2}{6}\partial_m((\rho c)^2\partial_m u) + \cdots, \\ p^* = p_0^n - \frac{\Delta t}{2}(\rho c)^2\partial_m u + \frac{\Delta t^2}{6}((\rho c)^2\partial_{mm}^2 p + 2\rho\mathscr{G}(\rho c)^2(\partial_m u)^2) + \cdots, \\ (pu)^* = (pu)_0^n - \frac{\Delta t}{2}(u(\rho c)^2\partial_m u + p\partial_m p) + \frac{\Delta t^2}{6}(u(\rho c)^2\partial_{mm}^2 p \\ \qquad +2\rho\mathscr{G}u(\rho c)^2(\partial_m u)^2 + 2(\rho c)^2(\partial_m u)(\partial_m p) + p\partial_m((\rho c)^2\partial_m u)) + \cdots. \end{cases} \tag{39}$$

These relations are used to build a second- and third-order accurate Lax-Wendroff-type scheme [24]. For convenience, we introduce $\bar{\psi}_{j+\frac{1}{2}}$ the mean value of ψ_j and ψ_{j+1} defined by

$$\overline{\psi}_{j+\frac{1}{2}} = \frac{1}{2}(\psi_j + \psi_{j+1}). \tag{40}$$

Second-order numerical fluxes

Let us define

$$\varphi_0^n = \frac{1}{2}(\varphi_j^n + \varphi_{j+1}^n) \text{ for } \varphi = u,\ p \quad \text{and} \quad pu. \tag{41}$$

Together with the following numerical fluxes, the Godunov-type scheme (27) is proved to be formally second-order accurate in both space and time:

$$\begin{cases} u_{j+\frac{1}{2}}^{*,O2} = u_0^n - \dfrac{\Delta t}{2}\dfrac{p_{j+1} - p_j}{\Delta m_{j+\frac{1}{2}}}, \\ p_{j+\frac{1}{2}}^{*,O2} = p_0^n - \dfrac{\Delta t}{2}\overline{(\rho c)^2}_{j+\frac{1}{2}}\dfrac{u_{j+1} - u_j}{\Delta m_{j+\frac{1}{2}}}, \\ (pu)_{j+\frac{1}{2}}^{*,O2} = (pu)_0^n - \dfrac{\Delta t}{2}\left(\overline{(u(\rho c)^2)}_{j+\frac{1}{2}}\dfrac{u_{j+1} - u_j}{\Delta m_{j+\frac{1}{2}}} + \bar{p}_{j+\frac{1}{2}}\dfrac{p_{j+1} - p_j}{\Delta m_{j+\frac{1}{2}}}\right), \end{cases} \tag{42}$$

where u_0^n, p_0^n and $(pu)_0^n$ are given by (41) and nodal masses by (30). Indeed, using Taylor expansions, one finds that the truncature error on each equation is in $\mathscr{O}(\alpha\Delta t + \beta\Delta x)^3$. The proof is rather long and is not detailed here.

Remark 4. Instead of the above last component flux, one could also have taken $\widetilde{(pu)}^* = p^{*,O2}u^{*,O2}$. The resulting scheme would therefore be close to the one proposed by Kashiwa-Lee [26][6], but would not be *stricto sensu* second-order accurate.

Third-order numerical fluxes

Let us define

$$\varphi_0^n = \frac{7}{12}(\varphi_j^n + \varphi_{j+1}^n) - \frac{1}{12}(\varphi_{j-1}^n + \varphi_{j+2}^n) \text{ for } \varphi = u,\ p \quad \text{and} \quad pu. \tag{43}$$

Together with the following numerical fluxes, the Lagrangian scheme (27) is proved to be formally third-order accurate in the finite-difference sense, in both space and time:

[6] The hybridation between the first- and second-order fluxes differs, along with the choice of limiters (see below).

$$
\begin{cases}
u^{*,O3}_{j+\frac{1}{2}} = u^n_0 - \dfrac{\Delta t}{2}\dfrac{p_{j+1}-p_j}{\Delta m_{j+\frac{1}{2}}} + \dfrac{\Delta t^2}{6\Delta m_{j+\frac{1}{2}}}\left((\rho c)^2_{j+1}\dfrac{u_{j+2}-u_j}{\Delta m_{j+\frac{1}{2}}+\Delta m_{j+\frac{3}{2}}} - (\rho c)^2_j \dfrac{u_{j+1}-u_{j-1}}{\Delta m_{j-\frac{1}{2}}+\Delta m_{j+\frac{1}{2}}}\right),\\
p^{*,O3}_{j+\frac{1}{2}} = p^n_0 - \dfrac{\Delta t}{2}\overline{(\rho c)^2}_{j+\frac{1}{2}}\dfrac{u_{j+1}-u_j}{\Delta m_{j+\frac{1}{2}}} + \dfrac{\Delta t^2}{3}\overline{(\rho\mathscr{G}(\rho c)^2)}_{j+\frac{1}{2}}\left(\dfrac{u_{j+1}-u_j}{\Delta m_{j+\frac{1}{2}}}\right)^2\\
\qquad + \dfrac{\Delta t^2}{6\Delta m_{j+\frac{1}{2}}}\overline{(\rho c)^2}_{j+\frac{1}{2}}\left(\dfrac{p_{j+2}-p_j}{\Delta m_{j+\frac{1}{2}}+\Delta m_{j+\frac{3}{2}}} - \dfrac{p_{j+1}-p_{j-1}}{\Delta m_{j-\frac{1}{2}}+\Delta m_{j+\frac{1}{2}}}\right),\\
(pu)^{*,O3}_{j+\frac{1}{2}} = (pu)^n_0 - \dfrac{\Delta t}{2}\left(\overline{(u(\rho c)^2)}_{j+\frac{1}{2}}\dfrac{u_{j+1}-u_j}{\Delta m_{j+\frac{1}{2}}} + \bar{p}_{j+\frac{1}{2}}\dfrac{p_{j+1}-p_j}{\Delta m_{j+\frac{1}{2}}}\right)\\
\qquad + \dfrac{\Delta t^2}{6\Delta m_{j+\frac{1}{2}}}\overline{(u(\rho c)^2)}_{j+\frac{1}{2}}\left(\dfrac{p_{j+2}-p_j}{\Delta m_{j+\frac{1}{2}}+\Delta m_{j+\frac{3}{2}}} - \dfrac{p_{j+1}-p_{j-1}}{\Delta m_{j-\frac{1}{2}}+\Delta m_{j+\frac{1}{2}}}\right)\\
\qquad + \dfrac{\Delta t^2}{6\Delta m_{j+\frac{1}{2}}}\bar{p}_{j+\frac{1}{2}}\left((\rho c)^2_{j+1}\dfrac{u_{j+2}-u_j}{\Delta m_{j+\frac{1}{2}}+\Delta m_{j+\frac{3}{2}}} - (\rho c)^2_j\dfrac{u_{j+1}-u_{j-1}}{\Delta m_{j-\frac{1}{2}}+\Delta m_{j+\frac{1}{2}}}\right)\\
\qquad + \dfrac{\Delta t^2}{3}\overline{(\rho\mathscr{G}u(\rho c)^2)}_{j+\frac{1}{2}}\left(\dfrac{u_{j+1}-u_j}{\Delta m_{j+\frac{1}{2}}}\right)^2 + \dfrac{\Delta t^2}{3}\overline{(\rho c)^2}_{j+\frac{1}{2}}\left(\dfrac{u_{j+1}-u_j}{\Delta m_{j+\frac{1}{2}}}\right)\left(\dfrac{p_{j+1}-p_j}{\Delta m_{j+\frac{1}{2}}}\right),
\end{cases}
\tag{44}
$$

where u^n_0, p^n_0 and $(pu)^n_0$ are given by (43). The proof has been established using a symbolic computation software and is not detailed here.

Remark 5. If the terms in (44) involving the fundamental derivative $\mathscr{G}$ are dropped, the resulting scheme is no longer third-order accurate on smooth flows.

Limiting procedures

These high-order numerical fluxes must be connected to first-order ones to correctly treat discontinuities. This is done *via* a limiter φ:

$$
\begin{cases}
u^{*,lim}_{j+\frac{1}{2}} = u^{*,O1}_{j+\frac{1}{2}} + \varphi_{j+\frac{1}{2}}\left(u^{*,ON}_{j+\frac{1}{2}} - u^{*,O1}_{j+\frac{1}{2}}\right),\\
p^{*,lim}_{j+\frac{1}{2}} = p^{*,O1}_{j+\frac{1}{2}} + \varphi_{j+\frac{1}{2}}\left(p^{*,ON}_{j+\frac{1}{2}} - p^{*,O1}_{j+\frac{1}{2}}\right),\\
(pu)^{*,lim}_{j+\frac{1}{2}} = p^{*,O1}_{j+\frac{1}{2}}u^{*,O1}_{j+\frac{1}{2}} + \varphi_{j+\frac{1}{2}}\left((pu)^{*,ON}_{j+\frac{1}{2}} - p^{*,O1}_{j+\frac{1}{2}}u^{*,O1}_{j+\frac{1}{2}}\right),
\end{cases}
$$

where the first-order numerical fluxes are given by (28) and the second ($N=2$) or third ($N=3$) ones are respectively given by (42) and (44). It remains to detail the limiter φ. By analogy with the usual artificial viscosity formulation, one may choose a limiting procedure based only on the velocity field, introducing

$$
\begin{cases}
\Delta u^*_j = \dfrac{u^*_{j+\frac{1}{2}} - u^*_{j-\frac{1}{2}}}{\Delta m_j},\\
\Delta u_{j+\frac{1}{2}} = \dfrac{u_{j+1}-u_j}{\Delta m_{j+\frac{1}{2}}},
\end{cases}
\quad\text{and}\quad
\begin{cases}
r^-_{j+\frac{1}{2}} = \dfrac{\Delta u^*_j}{\Delta u_{j+\frac{1}{2}}},\\
r^+_{j+\frac{1}{2}} = \dfrac{\Delta u^*_{j+1}}{\Delta u_{j+\frac{1}{2}}}.
\end{cases}
$$

Various limiters can therefore be defined. In the following sections, we will use

$$
\varphi_{j+\frac{1}{2}} = \max\left(0, \min\left(1, r^-_{j+\frac{1}{2}}, r^+_{j+\frac{1}{2}}\right)\right), \text{ the Minmod limiter,} \tag{45a}
$$

$$
\varphi_{j+\frac{1}{2}} = \max\left(0, \min\left(1, 2r^-_{j+\frac{1}{2}}, 2r^+_{j+\frac{1}{2}}, \frac{r^-_{j+\frac{1}{2}} + r^+_{j+\frac{1}{2}}}{2}\right)\right), \text{ the van Leer limiter.} \tag{45b}
$$

To benefit from *upwind limiting*, one may also choose another procedure based on the linearized Riemann invariants as was done in Section 5.2.3, defining

$$
\begin{cases}
J^{+,ON}_{j+\frac{1}{2}} = u^{*,ON}_{j+\frac{1}{2}} + (\rho c)^{-1}_j p^{*,ON}_{j+\frac{1}{2}},\\
J^{-,ON}_{j+\frac{1}{2}} = u^{*,ON}_{j+\frac{1}{2}} - (\rho c)^{-1}_{j+1} p^{*,ON}_{j+\frac{1}{2}},
\end{cases}
$$

and enforcing these fluxes to lie in the TVD or MP intervals, respectively defined by (35a), (35b) and (36a), (36b). The limited values $p^{*,lim}_{j+\frac{1}{2}}$ and $u^{*,lim}_{j+\frac{1}{2}}$ are then obtained by solving the linear system (34). If $J^{\pm,ON}_{j+\frac{1}{2}} \neq J^{\pm,lim}_{j+\frac{1}{2}}$ we set $(pu)^{*,lim}_{j+\frac{1}{2}} = p^{*,lim}_{j+\frac{1}{2}}.u^{*,lim}_{j+\frac{1}{2}}$. Whereas

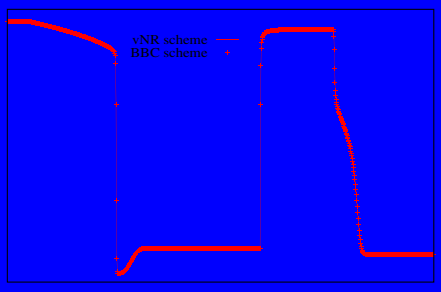

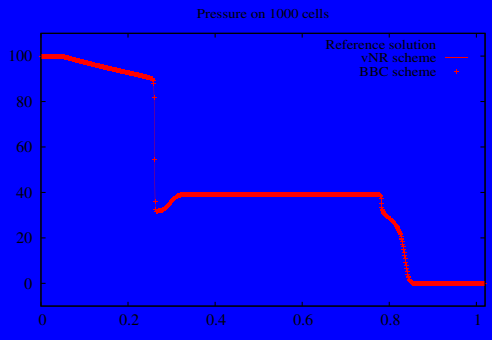

vNR and BBC schemes: "Magical" q (24)

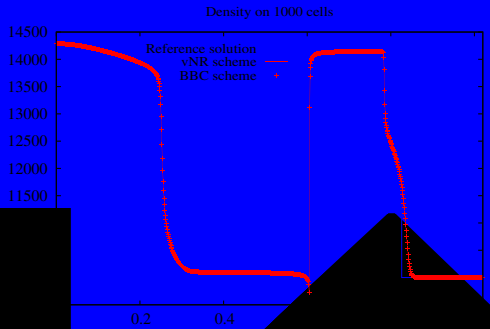

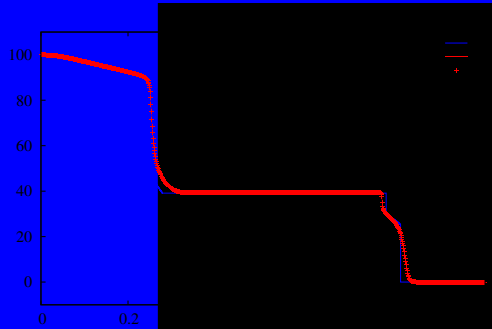

t problem at $t = 8$ … the vNR (lines) and B … (21)–(24)
… $c_l = 1$ (Density i…

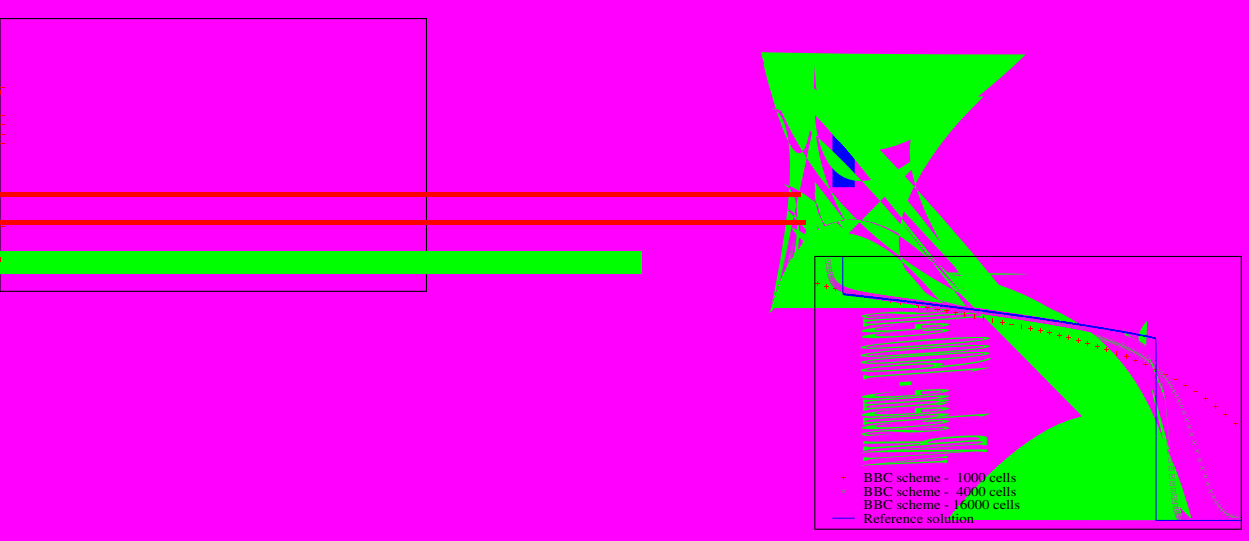

vNR and BBC schemes: "Magical" q (24)

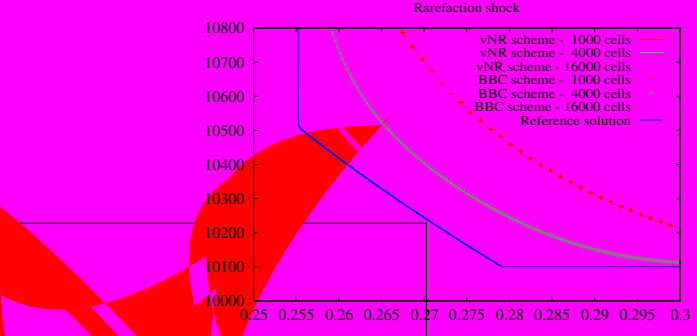

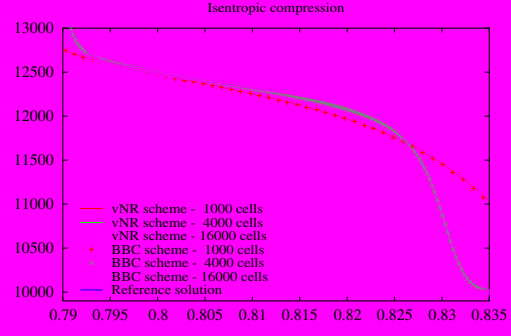

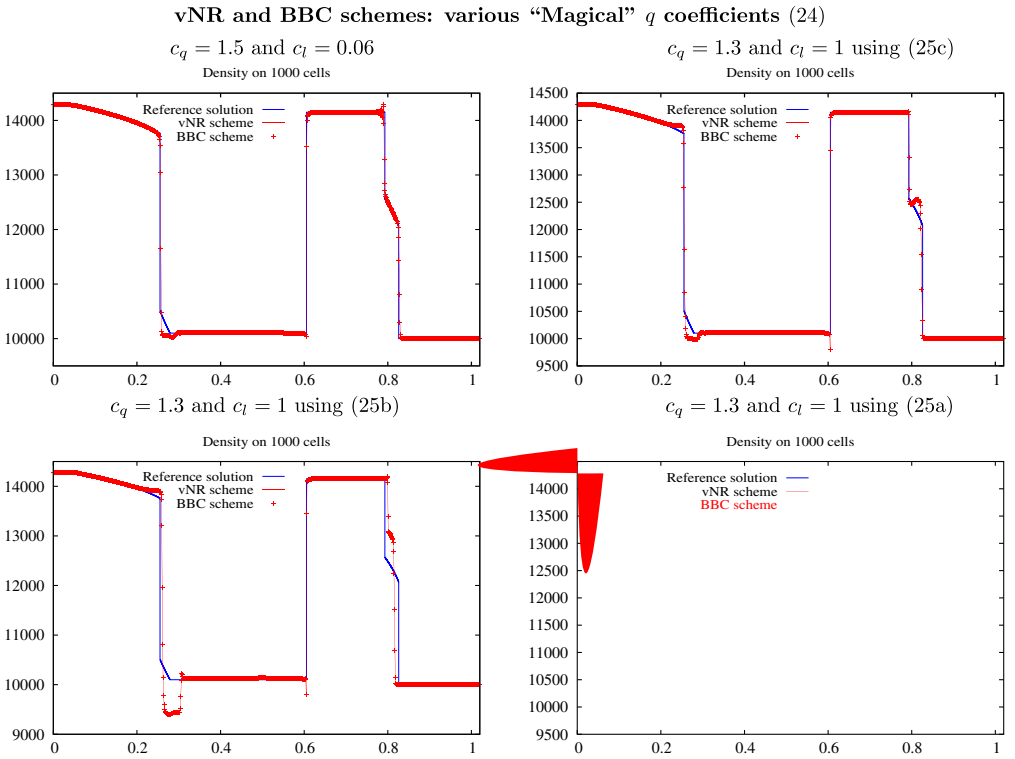

Fig. 6. Same as Fig. 4 with variants around the artificial viscosity (24). The Christensen's improvement (see Section 5.1.3) is used with limiters (25a) (bottom right), (25b) (bottom left) and (25c) (top right).

6. Numerical results

The various Lagrangian numerical schemes reviewed in Section 5 are now evaluated on the Bizarrium test problem defined in Section 4. For all the following graphs, the CFL number is fixed to 0.3 for vNR-type schemes and 0.6 for Godunov-type ones. Results are plotted at time $t = 8 \times 10^{-5}$ s.

6.1. vNR-type schemes

Density and pressure profiles obtained using the vNR and the BBC schemes on 1000 cells are plotted in Fig. 4. A zoom on the density around the rarefaction shock feet and the isentropic compression, for three different meshes (1000, 4000 and 16,000 cells) is also plotted in Fig. 5 for both schemes. In each case, the four artificial viscosities formulations (21)–(24) have been tested. As in [28,39,50], the quadratic and linear coefficients have been set to $c_q = 4$ and $c_l = 1$.

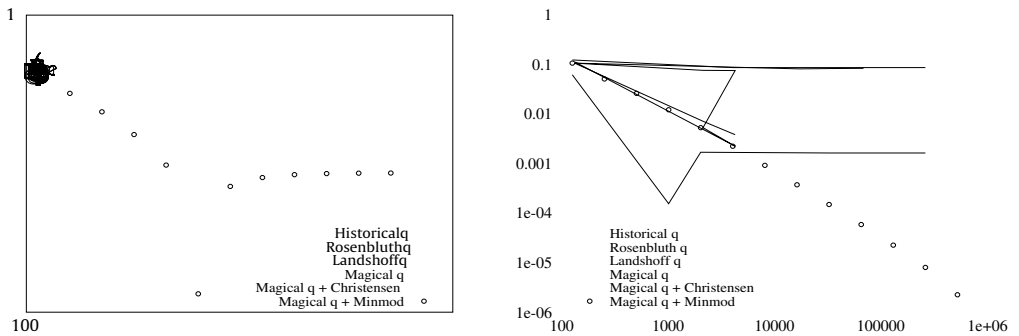

Fig. 7. Bizarrium test problem: vNR-type schemes. Error $Err(p_{CD})$ in GPa vs. the number of cells (see (46)).

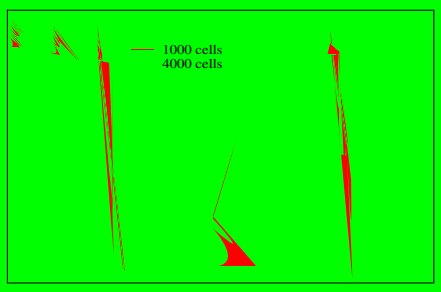

Second- and third-order CoHy schemes without limiter

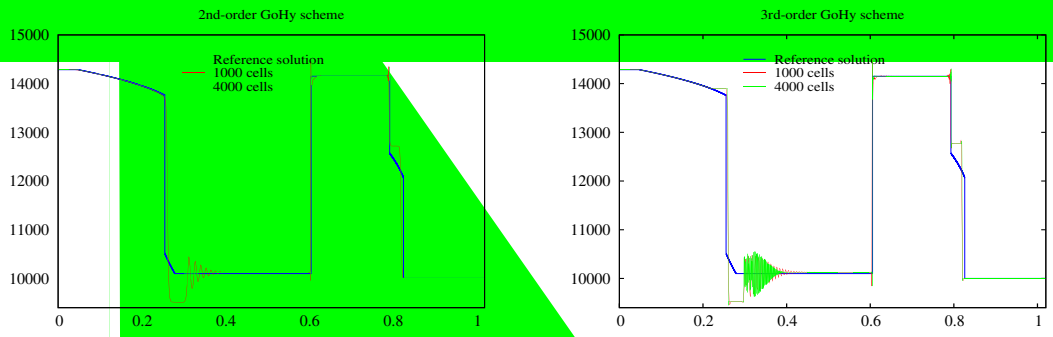

Fig. 8. Bizarrium test problem at $t = 8 \times 10^{-5}$ s (CFL = 0.6), using the first-order Godunov-type scheme, the second-order GAD, GAIA and GoHy schemes and the third-order GAIA and GoHy schemes without limiters. (Density in kg/m^3) and pressure in GPa).

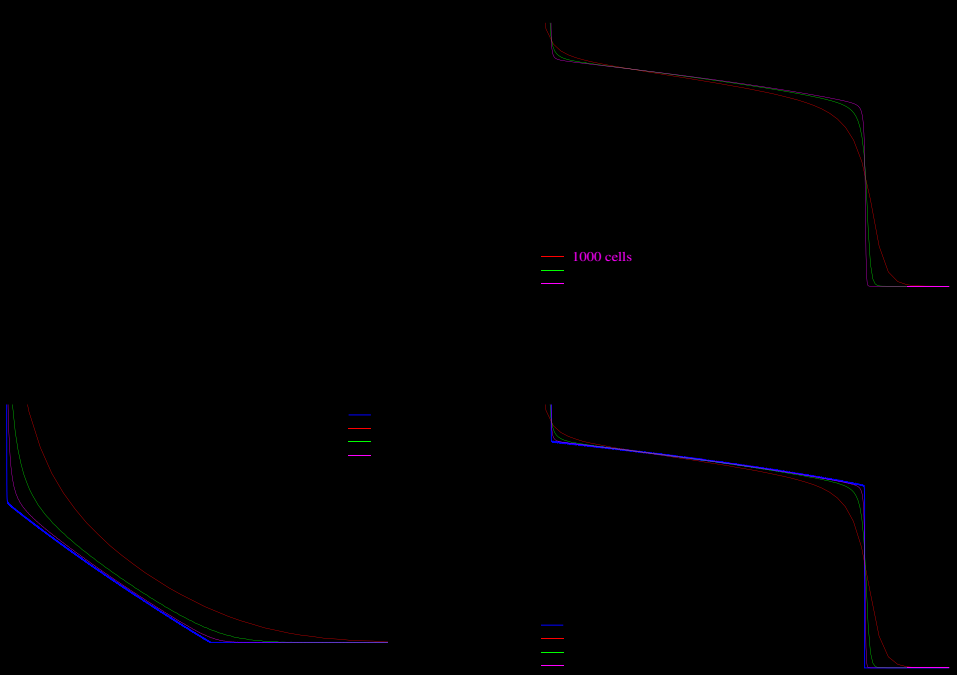

F 9. B za
d ity ar

These figures show that vNR and BBC results are very close at the first sight and lead to the following conclusions.

1. The rarefaction shock is not captured when using the Rosenbluth (22) or Landshoff (23) q formulations. This is due to the fact that q is set to zero in expansive waves.

Table 3
Total energy balance: relative error $|\frac{E(t=8\times10^{-5})-E(0)}{E(0)}|$ with $E(t)=\int_0^M e(m,t)dm$, for the vNR and the BBC schemes using the Magical q combination ($c_q=4$ and $c_l=1$).

nb cells	vNR scheme using (47a)	vNR scheme using (47b)	BBC scheme using (19)
2000	1.77473e−05	2.66159e−05	5.92283e−16
4000	2.50355e−05	2.75073e−05	2.96142e−15
8000	2.22746e−05	2.46182e−05	9.87146e−15
16,000	2.67333e−05	2.60038e−05	2.60605e−14

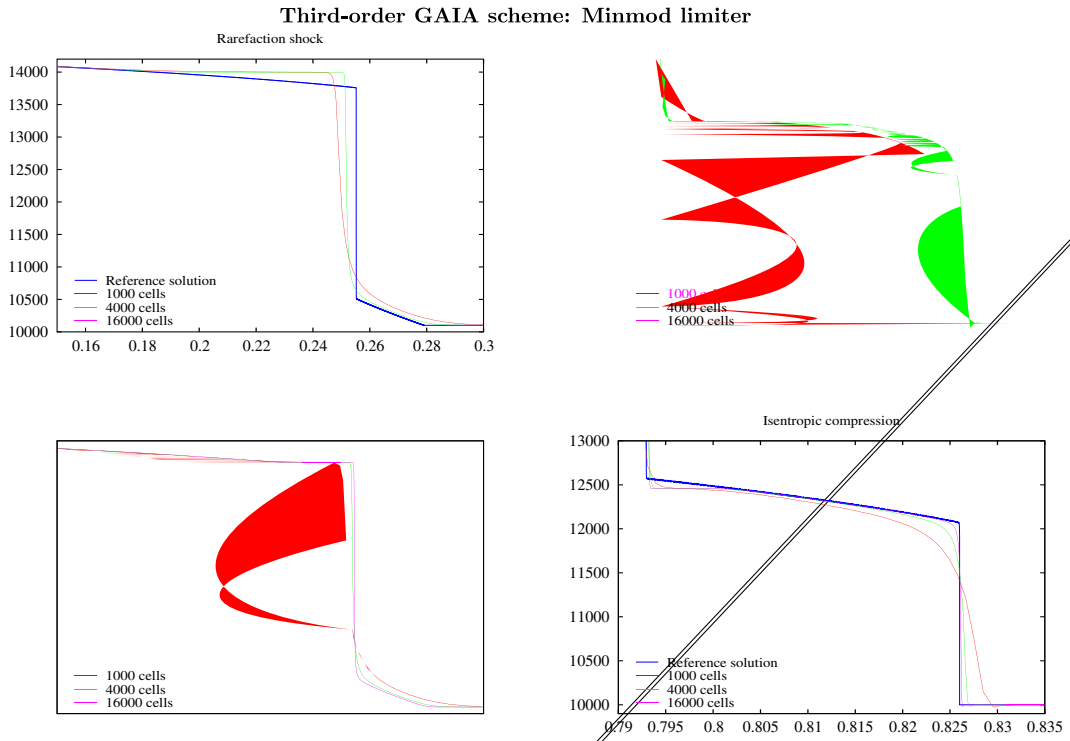

Fig. 11. Bizarrium test problem at $t=8\times10^{-5}$ s (CFL = 0.6), using the third-order GAIA and GoHy schemes with the Minmod limiter. Zoom on the density around the rarefaction shock feet (left) and the isentropic compression (right).

2. The rarefaction shock as well as the isentropic compression are not captured when using the von Neumann–Richtmyer (21) q formulation: a linear viscosity seems to be necessary to correctly compute composite waves.

Among all q formulations that have been tested, the "Magical" q combination is the only one which satifies these requirements. This is therefore the one we have retained for Fig. 6. In previous computations, we have set $c_q=4$ and $c_l=1$, which are greater values than those commonly used: according to [4], standard quadratic and linear coefficients are respectively $c_q=1.5$ and $c_l=0.06$. Fig. 6 (top-left) clearly shows that this set of parameters does not work. In particular, the linear coefficient is too small. Indeed, we have checked that with $c_q=1.3$ and $c_l=1$, which are parameters recommended in [4, p. 277] for the second-order estimations of Δu in the q computation, results were qualitatively similar to those obtained setting $c_q=4$ and $c_l=1$. The vNR and BBC schemes together with a second-order estimation of Δu (see Section 5.1.3) have therefore been evaluated with this set of coefficients. Density profiles obtained with limiters (25a)–(25c) are also given in Fig. 6, which shows that the Minmod limiter (which is the most dissipative one) is the only one which seems to work. Together with the fact that c_l must be sufficiently large[7], this seems to tell that numerical dissipation is the key point when dealing with non-convex EOS.

Remark 6. A more general formulation of (24) with quadratic term activated in both compression and expansion, $q=-c_q\rho\Delta u|\Delta u|-c_l\rho c\Delta u$, gives similar results. Since such a formulation is more dissipative than (24), the physically stable solution is also captured, including with Christensen's improvement when Minmod-limited. Nevertheless, it does not lead to qualitatively better results than those of Fig. 6 with (25b) and (25c) since the artificial dissipation in compressive waves is strictly the same.

[7] As was said in Section 5.1.3, the quadratic viscosity concentrates numerical dissipation near the shock front while the linear one has a more diffuse effect.

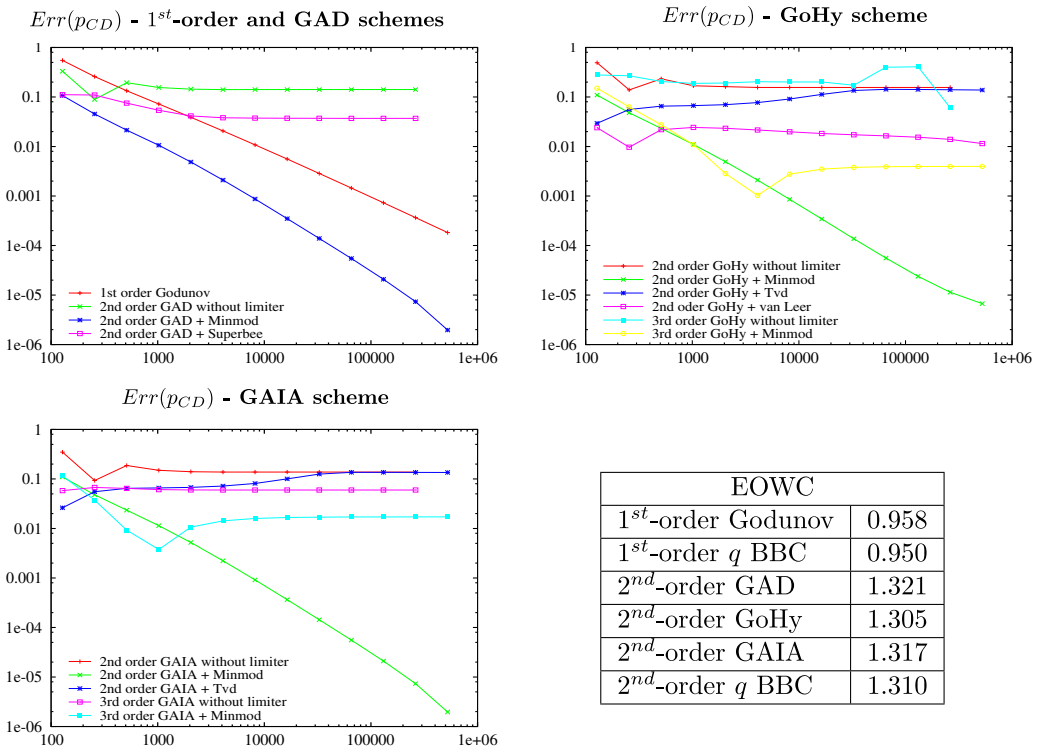

EOWC	
1^{st}-order Godunov	0.958
1^{st}-order q BBC	0.950
2^{nd}-order GAD	1.321
2^{nd}-order GoHy	1.305
2^{nd}-order GAIA	1.317
2^{nd}-order q BBC	1.310

Fig. 12. Bizarrium test problem: Godunov-type schemes. Error $Err(p_{CD})$ in GPa vs. the number of cells (see (46)). Bottom right: experimental order of weak convergence (EOWC) for all the *working* schemes.

A weak convergence study has also been performed. We have chosen to evaluate the mean pressure around the contact discontinuity and to compare it to its theoretical value $p^{exact} = p_{yz} = p_{zy}$ (given in Table 2). Let x_{CD} denote the position of the contact discontinuity and let $x_G = x_{CD} - 0.05$ and $x_D = x_{CD} + 0.05$. Corresponding mass coordinates are denoted m_G and m_D. The measure of the error is defined by

$$Err(p_{CD}) \stackrel{\text{def}}{=} \left| p^{exact} - \frac{1}{m_D - m_G} \int_{m_G}^{m_D} p^{num} dm \right|. \tag{46}$$

This error is plotted in Fig. 7 for the vNR and the BBC schemes, for meshes of $128 * 2^k$ cells (k varying from 0 to 12).

As expected, the von Neumann–Richtmyer, Rosenbluth and Landshoff q formulations, as well as the Magical q one with a Christensen limited second-order evaluation of Δu, fail to converge to the exact solution (with both vNR and BBC schemes). But these graphs contain additional informations: even with the Magical q formulation, the vNR scheme fails to converge. We infer that this is due to non-conservation of total energy, which is a well-known deficiency of the vNR scheme[8]: see Table 3 where the relative error on the total energy balance is reported, using

$$e_j^n = \varepsilon_j^n + \frac{1}{8}\left(u_{j-\frac{1}{2}}^{n-\frac{1}{2}} + u_{j+\frac{1}{2}}^{n-\frac{1}{2}}\right)^2 \text{ following } [14, 33] \text{ or} \tag{47a}$$

$$e_j^n = \varepsilon_j^n + \frac{1}{8}\left(u_{j-\frac{1}{2}}^{n-\frac{1}{2}} + u_{j+\frac{1}{2}}^{n-\frac{1}{2}}\right)\left(u_{j-\frac{1}{2}}^{n+\frac{1}{2}} + u_{j+\frac{1}{2}}^{n+\frac{1}{2}}\right) \text{ following } [45]. \tag{47b}$$

This intuition is strengthened by the BBC scheme results for which all tested q formulations also fail to converge, except the Magical q combination with an appropriate set of coefficients. A second-order accurate evaluation of Δu then does work, but with a dissipative limiter (Minmod). The BBC scheme's success is attributed to the discrete conservation of total energy (Table 3).

6.2. Godunov-type schemes

Density profiles obtained with the various Godunov-type schemes presented in Section 5.2 are plotted in Figs. 8–11. Fig. 8 shows that the first-order Godunov-type scheme recalled in Section 5.2.1 seems to capture the physical solution, in contrast to all the presented high-order extensions without limiters. This defect is corrected for second-order extensions by using the

[8] See also the *much simpler* plane infinite shock problem of Noh [36] to illustrate such a deficiency.

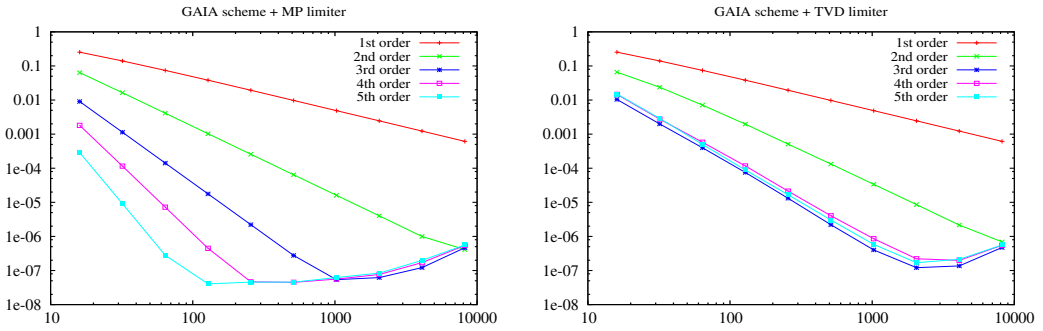

	Experimental Order of Convergence (EOC)				
	1^{st}-order	2^{nd}-order	3^{rd}-order	4^{th}-order	5^{th}-order
GAIA - no limiter	0.988	1.997	3.001	3.996	4.986
GAIA - MP		1.997	3.002	4.002	5.004
GAIA - TVD		1.794	2.363	2.283	2.511
GAIA - Minmod		1.228	1.262	1.273	1.265
GoHy - no limiter		1.997	3.017	4.001	
GoHy - MP		1.996	3.017	3.997	
GoHy - TVD		1.794	2.107	2.283	
GoHy - Minmod		1.432	1.397	1.389	
GAD - no limiter		1.997			
GAD - Minmod		1.315			
GAD - Superbee		1.096			

Fig. 13. Acoustic wave propagation test problem: experimental order of convergence (EOC) for the three Godunov-type schemes with (and without) the presented limiters.

Minmod limiter (Fig. 9). All other standard limiters (superbee, TVD, MP or van Leer) are not dissipative enough to correctly capture composite waves[9] (Fig. 10) and even when Minmod-limited, both third-order extensions fail on the Bizarrium test problem (Fig. 11).

The same weak convergence study as the one performed in the previous section confirms these facts. The error on the mean value of the contact discontinuity pressure $Err(p_{CD})$ is plotted in Fig. 12. The first-order Godunov-type scheme (27–28) converges to the reference solution without any *ad hoc* numerical coefficient as well as the second-order GAD, GAIA and GoHy extensions with the Minmod limiter. With the other basic limiters presented in Section 5.2 (which are less dissipative), the physical solution is not captured. Both GAIA and GoHy third-order extensions also fail with these limiters. As with vNR-type schemes, these results indicate that in order to capture the physical solution, such Godunov-type schemes must provide an appropriate level of numerical dissipation.

7. Conclusion

A thermodynamically consistent non-convex EOS that can be easily introduced in Eulerian as well as Lagrangian hydrocodes for test purposes has been proposed, along with a reference solution for an initial value problem exhibiting a complex composite wave pattern (Bizarrium Riemann problem). The solution consists in a left-facing expansive composite wave (rarefaction/rarefaction shock/rarefaction) and a right-facing compressive composite one (shock/sonic isentropic compression/shock) separated by a contact discontinuity. In contrast to the standard theory (convex EOS), the entropy condition is not sufficient to guarantee uniqueness of solutions to Riemann problems and one has to resort to the Liu-Oleinik criterion (existence of viscous profiles). This suggests that numerical schemes require strong enough dissipation to capture the admissible solution. This point has been numerically examined.

Two standard Lagrangian shock capturing approaches, both based on a finite volume method, have been recalled (vNR and Godunov-type schemes) and evaluated on the Bizarrium test problem. In particular, a complete description of several *state-of-the-art* high-order Godunov-type schemes applicable to general EOSs has been provided.

The vNR Lagrangian scheme fails on that problem, most probably due to the fact that the total energy is not conserved with this scheme, whereas the unstaggered in time *conservative* BBC version reveals satisfactory, using a particular (and somehow unusual) artificial viscosity formulation, with linear viscosity activated on both compression and *expansion* waves. To improve shock resolution, the common practice of a second-order accurate evaluation of Δu in the computation of the artificial viscosity then does work, but with a dissipative limiter (Minmod). In a word, this particular vNR-type scheme, extendable to nD Cartesian grids *via* 1D remapping and directional splitting, does converge provided it contains strong enough numerical dissipation.

[9] The MP intervals (36a) include the TVD ones (35a) (see Section 5.2.3).

Concerning Godunov-type schemes, a noticeable fact is that the first-order Lagrangian scheme based on the *acoustic* Riemann solver the converges without any *ad hoc* numerical coefficient. On the other hand, the three very different second-order extensions presented do work using the Minmod limiter. With the other basic and standard limiters presented, the physical solution is not captured. Moreover, third-order extensions (and higher-order ones also) fail with all the limiters considered. This deficiency is attributed to the low level of numerical dissipation, unable to capture the viscous profile of the composite wave pattern.

Quite severe when working on high-order schemes, this Riemann problem appears as a challenging benchmark for devising new limiters and/or next-generation highly accurate schemes.

This study has been conducted in the context of *hydrodynamics*, most notably relative to the choice of the non-convex EOS and the classes of numerical schemes considered. We infer that the proposed benchmark could also be valuable to the compressible *gas dynamic* community, provided numerical solvers handle general EOSs.

Appendix A. High-order accuracy estimations

Since the Bizarrium test problem involves shock waves, it does not allow a measure of the effective accuracy of a scheme and must be used conjointly to more academic smooth-flow test problems. Two of them are recalled in the following sections and used to evaluate the effective order of the various Godunov-type schemes described in Section 5.2. We also include results obtained with the fourth-order GoHy scheme which has not been detailed in this paper.

A.1. Linear acoustic wave limit of the Euler equations

Let ε be a small parameter, and $(\rho, u, p)_0^\varepsilon$ the initial condition, defined by

$$\begin{cases} \rho_0^\varepsilon = \rho_0^0 + \varepsilon \sin(kx), \\ u_0^\varepsilon = \varepsilon \sin(kx), \\ p_0^\varepsilon = p_0^0 + \varepsilon \sin(kx), \end{cases}$$

where ρ_0^0 and p_0^0 are constant unperturbed values. It can then be easily shown that

$$\begin{cases} \rho^\varepsilon(x,t) = \rho_0^0 + \varepsilon \sin(k(x-t)), \\ u^\varepsilon(x,t) = \varepsilon \sin(k(x-t)), \\ p^\varepsilon(x,t) = p_0^0 + \varepsilon \sin(k(x-t)), \end{cases}$$

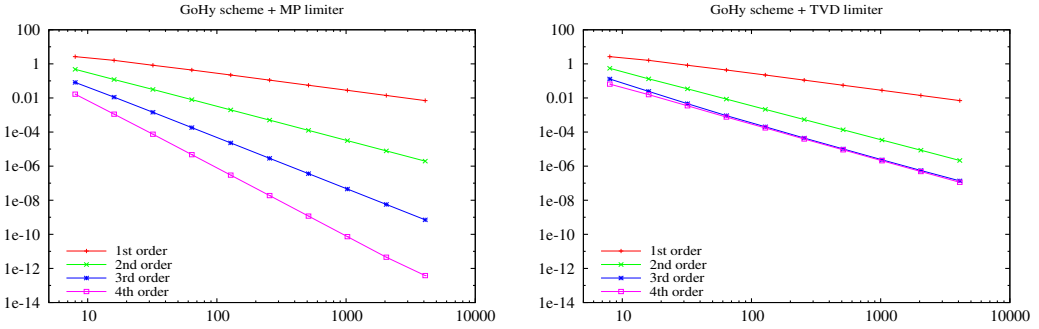

Experimental Order of Convergence (EOC)			
1^{st}-order	2^{nd}-order	3^{rd}-order	4^{th}-order

GAIA - no limite

is solution to the linearized gas dynamics equations. The system is closed with a perfect gas EOS, whose adiabatic exponent is $\gamma = 7/5$. The length of the computational domain is equal to 1, and we set $k = 2\pi$, $\rho_0^0 = 1$ and $p_0^0 = 5/7$, so that the acoustic wave propagates at speed $c = 1$. Periodic boundary conditions have been used. The error which has been measured here is the L^1 norm of the velocity deviation away from the above exact solution after one revolution (thus at time $t = 1$), divided by ε which has been set to 10^{-8}.

The GAD, GoHy and GAIA schemes have been tested, without limiters as well as with the ones described in Section 5.2. Results are given in Fig. 13. Theoretical accuracy orders are almost recovered for all schemes without limiter, as well as for the GAIA and GoHy ones when MP-limited. Note that the limit of the linear regime is reached with the 5th-order GAIA-MP scheme with 128 cells.

A.2. Strong isentropic compression

Now we consider the planar Kidder's test problem [27], which consists in the isentropic compression of a perfect gas whose adiabatic exponant is $\gamma = 3$. The initial condition is given by:

$$\begin{cases} \rho(X,0) = \left(\frac{\rho_e^{\gamma-1}X^2 + \rho_i^{\gamma-1}(L^2-X^2)}{L^2}\right)^{\frac{1}{\gamma-1}}, \\ u(X,0) = 0, \\ p(X,0) = p_e\left(\frac{\rho}{\rho_e}\right)^{\gamma}, \end{cases}$$

with $L = 1$, $p_e = 100$, $\rho_e = 1$ and $p_i = 1$. From the isentropic condition $p_i\rho_i^{-\gamma} = p_e\rho_e^{-\gamma}$ we get the initial value for ρ_i. We impose a wall boundary condition at $X = 0$ and the pressure law $p(x_e,t) = p_e h(t)^{-\gamma}$ on the external surface $x_e = x(X = L,t)$. Here $h(t)$ is the self-similar motion law, i.e. $x(X,t) = Xh(t)$, defined by

$$h(t) = \sqrt{1 - \frac{t^2}{t_c^2}} \text{ with } t_c = \sqrt{\frac{1}{2\gamma}\frac{L^2}{\varepsilon_e - \varepsilon_i}},$$

t_c being the collapse time and ε the internal energy. The self-similar solution is therefore given by

$$\begin{cases} \rho^{ex}(x,t) = \frac{1}{h(t)}\ \rho\left(\frac{x}{h(t)},0\right), \\ u^{ex}(x,t) = -\frac{x\ t}{t_c^2 h(t)^2}, \\ p^{ex}(x,t) = p_e\left(\frac{\rho^{ex}(x,t)}{\rho_e}\right)^{\gamma}. \end{cases}$$

The experimental order of convergence has been measured on the L^1 norm of $U - U^{ex}$ where $U = (\tau,u,e)^t$ at time $t = 0.5t_c$. Results are given in Fig. 14. As expected, third- and fourth-order accuracy is not recovered with the GAIA scheme on the full nonlinear Euler equations. Theoretical orders are recovered with the GoHy scheme without limiter or when MP-limited.

References

[1] G.B. Alalikin, S.K. Godunov, I.L. Kireeva, L.A. Pliner. Resolution of one-dimensional problems of gas dynamics with moving meshes, Moscow, Naouka, 1970 (in Russian).
[2] S.M. Bakhrakh, G.V. Zharova, V.F. Spiridinov, A conservative scheme for the computation of axisymmetric flows (an explicit–implicit algorithm), Voprosy Atomnoi Nauki I Tekhniki. Ser. Math. Model. Phys. Process. 3 (1982) 15–21 (in Russian).
[3] I. Bazarov, Thermodynamique, Mir Moscou, 1989 (in French).
[4] D.J. Benson, Computational methods in Lagrangian and Eulerian hydrocodes, Comput. Meth. Appl. Mech. Eng. 99 (1992) 235–394.
[5] H. Bethe, The theory of shock waves for an arbitrary equation of state, Technical Report PB-32189, Clearinghouse for federal scientific and technical information, US Department of commerce, Washington, DC, 1942.
[6] H.B. Callen, Thermodynamics and an introduction to thermostatistics, second ed., John Wiley and Sons, 1985.
[7] M.S. Cramer, Shock splitting in single-phase gases, J. Fluid Mech. 199 (1989) 281–296.
[8] M.S. Cramer, R. Sen, Exact solutions for sonic shocks in Van der Waals gases, Phys. Fluids 30 (2) (1987) 377–385.
[9] W. Dahmen, S. Müller, A. Voss, Riemann problem for the Euler equations with non-convex equation of state including phase transition, in: G. Warnecke (Ed.), Analysis and Numerics for Conservation Laws, Springer, Berlin, 2005, pp. 137–162.
[10] V. Daru, C. Tenaud, High-order one-step monotonicity-preserving schemes for unsteady compressible flow calculations, J. Comput. Phys. 193 (2004) 563–594.
[11] J.-C. Desgraz, Le schéma "Godunov Anti-Diffusé", Unpublished work.
[12] B. Després, C. Mazeran, Lagrangian gas dynamics in two dimensions and Lagrangian systems, Arch. Rational Mech. Anal. 178 (2005) 327–372.
[13] J.K. Dukowicz, A general, non-iterative Riemann solver for Godunov's method, J. Comp. Phys. 61 (1985) 119–137.
[14] J.E. Fromm, Lagrangian difference approximation for fluid dynamics, Technical Report LA-2535, Los Alamos Scientific Laboratory, 1961.
[15] S.K. Godunov, A finite difference method for the numerical computation of discontinuous solutions of the equations of fluid dynamics, Math. Sb. 47 (1959) 271–306 (in Russian).
[16] S.K. Godunov, Reminiscences about difference schemes, J. Comp. Phys. 153 (1999) 6–25.
[17] S.K. Godunov, A.V. Zabrodin, M.Ya. Ivanov, A.N. Kraiko, G.P. Prokopov. Résolution Numérique des Problèmes Multidimensionnels de la Dynamique des Gaz, Moscou, Ed. Mir, 1979 (in French).
[18] S.K. Godunov, A.V. Zabrodin, G.P. Prokopov, A computational scheme for two-dimensional non-stationary problems of gas dynamics and calculation of the flow from a shock wave approaching a stationay state, USSR Comput. Maths Math. Phys. 1 (1961) 1187–1219 (in Russian).

[19] O. Heuzé, Propagation des ondes mécaniques dans des milieux à isentropes changeant de concavité, Note CEA R-6146, ISSN 0429-3460, CEA, 2007 (in French).
[20] O. Heuzé, S. Jaouen, H. Jourdren, Wave propagation in materials with non-convex equations of state, in: M. Elert et al. (Eds.), Shock Compression of Condensed Matter – 2007: Proceedings of the Conference of the American Physical Society Topical Group on Shock Compression of Condensed Matter, Waikoloa (Hawaii), 24–29 June 2007. AIP Conf. Proc. vol. 955, pp. 47–50.
[21] O. Heuzé, S. Jaouen, H. Jourdren, Wave propagation in non monotonous sound speed materials, in: Europyro-07/34th IPS Conference, Beaune, October 8–11, 2007, pp. 339–346.
[22] S. Jaouen, Étude mathématique et numérique de stabilité pour des modèles hydrodynamiques avec transition de phase, Thèse de doctorat, Université Paris 6, 2001.
[23] E. Jouguet, Remarques sur la loi adiabatique d'Hugoniot, C.R. Acad. Sci. Paris 139 (1904) 786–789.
[24] H. Jourdren, Le schéma "Godunov hybride", Unpublished work.
[25] H. Jourdren, HERA: a hydrodynamic AMR platform for multi-physics simulations, in: Plewa Tomasz et al. (Eds.), Adaptative Mesh Refinement – Theory and Applications, Proceedings of the Chicago workshop on adaptative mesh refinement methods, Chicago, IL, USA, September 3–5, 2003, vol. 41 of Lecture Notes in Computational Science and Engineering, Springer, Berlin, 2005, pp. 283–294.
[26] B. Kashiwa, W.H. Lee, Comparisons between the cell-centered and staggered mesh Lagrangian hydrodynamics, in: Advances in the Free-Lagrange Method, Volume 395 of Lecture notes in Physics, Springer-Verlag, 1991, pp. 277–288.
[27] R.E. Kidder, Laser-driven compression of hollow shells: power requirements and stability limitations, Nuclear Fusion 1 (1976) 3–14.
[28] R. Landshoff, A numerical method for treating fluid flow in the presence of shocks, Technical Report LA-1930, Los Alamos Scientific Laboratory, 1955.
[29] P. Lax, Hyperbolic systems of conservation laws II, Commun. Pure Appl. Math. 10 (1957) 537–566.
[30] W.H. Lee, P.P. Whalen. Calculation of shock problems by using four different schemes, Technical Report LA-UR-84-344, Los Alamos National Laboratory, 1984.
[31] T.P. Liu, The Riemann problem for general systems of conservation laws, J. Diff. Eq. 18 (1975) 218.
[32] T.P. Liu, The entropy condition and the admissibility of shocks, J. Math. Anal. Appl. 53 (1976) 78.
[33] C.L. Mader, Numerical modeling of detonations, Los Alamos Series in Basic and Applied Sciences, University of California Press, 1979.
[34] R. Menikoff, B.J. Plohr, The Riemann problem for fluid flow of real materials, Rev. Modern Phys. 61 (1) (1989) 75–130.
[35] S. Müller, A. Voss, The Riemann problem for the Euler equations with nonconvex and nonsmooth equation of state: construction of wave curves, SIAM J. Sci. Comput. 28 (2) (2006) 651–681.
[36] W.F. Noh. Errors for calculations of strong shocks using an artificial viscosity and an artificial heat flux, Technical Report UCRL-53669, Lawrence Livermore National Laboratory, 1985.
[37] S. Del Pino, H. Jourdren, Arbitrary high-order schemes for the linear advection and wave equations: application to hydrodynamics and aeroacoustics, C.R. Acad. Sci. Paris 342 (2006) 441–446.
[38] Y.P. Popov, A.A. Samarskii, Completely conservative difference schemes, Zhurnal Vysshei Matematiki Matematicheskoi Fisiki 9 (4) (1969) 953–958 (in Russian).
[39] R.D. Richtmyer, K.W. Morton, Difference Methods for Initial-value Problems, second ed., Wiley-Interscience, 1967.
[40] B. Riemann, Gesammelte Werke (1876) 144 (in German).
[41] R. Smith, The Riemann problem in gas dynamics, Trans. Am. Math. Soc. 249 (1) (1979) 1–50.
[42] A. Suresh, H.T. Huynh, Accurate monotonicity-preserving schemes with Runge–Kutta time stepping, J. Comp. Phys. 136 (1997) 83–99.
[43] P.A. Thompson, A fundamental derivative in gasdynamics, Phys. Fluids 14 (9) (1971) 1843–1849.
[44] P.A. Thompson, K.C. Lambrakis, Negative shock waves, J. Fluid Mech. 60 (1973) 187–208.
[45] J.G. Trulio, K.R. Trigger, Numerical solution of the one-dimensional Lagrangian hydrodynamic equations, Technical Report UCRL-6267, Lawrence Radiation Laboratory, 1961.
[46] J. von Neumann, R.D. Richtmyer, A method for the numerical calculation of hydrodynamic shocks, J. Appl. Phys. 21 (1950) 232–237.
[47] B. Wendroff, The Riemann problem for materials with non-convex equations of state: I, Isentropic flow, J. Math. Anal. Appl. 38 (1972) 454–466.
[48] B. Wendroff, The Riemann problem for materials with non-convex equations of state: II, General flow, J. Math. Anal. Appl. 38 (1972) 640–658.
[49] H. Weyl, Shock waves in arbitrary fluids, Com. Pure Appl. Math. II 103 (1949) 103–122.
[50] M.L. Wilkins, Use of artificial viscosity in multidimensional fluid dynamic calculations, J. Comp. Phys. 36 (1980) 281–303.
[51] P. Woodward, P. Colella, The numerical simulation of two-dimensional fluid flow with strong shocks, J. Comp. Phys. 54 (1984) 115–173.
[52] Ya.B. Zel'dovich, Yu.P. Raizer, Physics of Shock Waves and High-temperature Hydrodynamic Phenomena, second ed., Academic Press, 1967.